January 2013

Thermal Infrared Reflective Metal Oxide Sol-Gel Coatings for Carbon Fiber Reinforced Composite Structures

Brandon Demar Richard
University of South Florida, brichard@mail.usf.edu

Thermal Infrared Reflective Metal Oxide Sol-Gel Coatings for Carbon Fiber Reinforced Composite Structures

by

Brandon Demar Richard

A dissertation submitted in partial fulfillment
of the requirements for the degree of
Doctor of Philosophy
Department of Electrical Engineering
College of Engineering
University of South Florida

Major Professor: Sylvia Thomas, Ph.D.
Norma Alcantar, Ph.D.
Sanjukta Bhanja, Ph.D.
Shekhar Bhansali, Ph.D.
Nydeia Bolden, Ph.D.
Andrew Hoff, Ph.D.
Theda Daniels-Race, Ph.D.

Date of Approval:
April 2, 2013

Keywords: Antimony, Tin Oxide, Cobalt, Laser Interaction, Aerospace

DEDICATION

To my parents, immediate and extended family, and friends for their support. Our accomplishments will forever be a testimony that faith and prayer changes things beyond our imagination.

ACKNOWLEDGMENTS

First, I would like to thank the fellowship programs and organizations that supported and funded my graduate school experience: the National Science Foundation – Bridge to Doctorate Program (BD), the Florida Education Foundation – McKnight Doctoral Fellowship, and the Alfred P. Sloan Doctoral Fellowship. I would like to thank my advisor, Dr. Sylvia Thomas, for her guidance and confidence in my success. A special thank you goes to my internal and external committee members for their guidance through the success of this research. Special thanks to my fellow colleagues in the AMBIR laboratory group of ENB 352. A special thanks goes to the Bridge to the Doctorate and McKnight Doctoral Fellows and program directors, advisors, and faculty. A special thanks goes to the technicians and engineers at the Nanotechnology Research and Education Center (NREC) for their assistance in fabrication and characterization. A huge thanks goes to the entire Air Force Research Laboratories at Eglin Air Force Base, especially Dr. Nydeia Bolden, Mr. David Edwards, Dr. Dennis Goldstein, Dr. Mario Fajardo, and Mrs. Virginia Swindell. Special thanks goes to three of my mentors who have assisted my personal and academic development: Dr. Theda Daniels-Race, Mrs. Vallerie Maurice, and Mrs. Mae Vernon for pushing me to pursue the highest level of education. To my Southern University A&M family, especially Frank Alexander, Jr. Justin Boone, and Eric Huey, the long nights in Pinchback Hall are continuing to pay off.

TABLE OF CONTENTS

LIST OF TABLES

LIST OF FIGURES

ABSTRACT

Recent trends in composite research include the development of structural materials with multiple functionalities. In new studies, novel materials are being designed, developed, modified, and implemented into composite designs. Typically, an increase in functionality requires additional material phases within one system. The presence of excessive phases can result in deterioration of individual or overall properties. True multi-functional materials must maintain all properties at or above the minimum operating limit. In this project, samples of antimony and cobalt-doped tin oxide (ATO(Co_2O_3)) sol-gel solutions are used to coat carbon fibers and are heat treated at a temperature range of 200 – 500 °C. Results from this research are used to model the implementation of sol-gel coatings into carbon fiber reinforced multifunctional composite systems. This research presents a novel thermo-responsive sol-gel/ (dopant) combination and evaluation of the actuating responses (reflectivity and surface heat dissipation) due to various heat treatment temperatures. While ATO is a well-known transparent conductive material, the implementation of ATO on carbon fibers for infrared thermal reflectivity has not been examined. These coatings serve as actuators capable of reflecting thermal infrared radiation in the near infrared wavelengths of 0.7-1.2 μm. By altering the level of Co_2O_3 and heat treatment temperatures, optimal optical properties are obtained. While scanning electron microscopy (SEM) is used for imaging, electron diffraction

spectroscopy (EDS) is used to verify the compounds present in the coatings. Fourier transform infrared (FT-IR) spectroscopy was performed to analyze the chemical bonds and reflectivity in the infrared spectra after the heat treatments. Total reflection and angle-dependent reflectivity measurements were performed on the coatings in the wavelengths of 0.7-2 μm. Laser induced damage threshold testing was done to investigate the dielectric breakdown and used to calculate surface temperatures.

CHAPTER 1

INTRODUCTION

1.1. Applications of Thermal Infrared Reflectivity

Infrared wavelengths can be used to detect and image a vast amount of objects in our daily environment. For military purposes, thermal infrared imaging can be used to sense various objects in dark areas. This imaging phenomenon is made possible from the thermal infrared radiation objects emit in free space. It is also from this phenomenon where understanding the use of infrared radiation to damage a surface comes from. In order to damage a surface in a specified amount of time, the infrared radiation of an object must be less than the radiation being used to damage it. Several other factors vary the required infrared radiation amount, such as altitude, distance from target, and elements between the targets (i.e., moisture, temperature change). In the effort of promoting stealth and increasing longevity of aerospace vehicles subjected to infrared radiation imaging and damage, a selection of coatings can be added to the structure. These coatings molecularly interact with infrared light to reflect or absorb the photons being emitted towards its surface. The surface chemistry dominates the interaction of infrared radiation on a surface of specified material. Therefore, a selected amount of lasers of designated wavelengths are used in specific applications. It is because of this

that the implementation of thermally reflective coatings occur in multiple areas of application. The selection, alteration, and functionalization of materials is critical to the success of high reflectivity from a specified material.

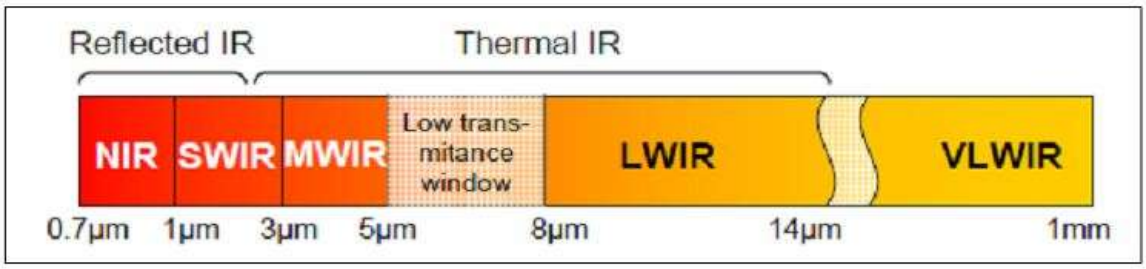

Figure 1.1.1. Infrared spectra from 0.7 to 1 millimeter.[1] (public domain)

Thermally reflective materials are investigated for their capability to withstand certain amounts of laser power at specified times. Infrared lasers operate in all bands of the infrared spectra – near, mid, and far infrared. Figure 1.1.1 shows the bandwidth for the infrared spectra. [2, 3] In the field of optics, materials are investigated for their capability to withstand certain amounts of laser powers at specified times. Laser degradation is a technique used to examine materials for their optical strength under laser radiation in applications such as optoelectronics[4], laser mirrors, and even telecommunications. Some variable parameters characterizing the degradation are laser intensity (J/cm^2), beam width (µm), pulse width or speed (ns), and power (watts). While laser power can reach hundreds of megawatts (MW), laser degradation experiments are usually done in the lower microwatt (µW) to milliwatt (mW) range. The operating wavelength of a laser depends on the materials inside the laser structure. For instance, a carbon dioxide (CO_2) gas laser operates at the 10 µm wavelength, while a Nd:YAG laser

operates at 1.06 μm (1064 nm). Laser wavelength also determines the pulse speed of the laser, meaning a laser can be continuous or pulsing at such a fast rate to where it appears to be continuous. Because lasers of different wavelengths, frequencies, and power are used in designated systems, materials containing a wide range of optical strength must be identified and employed for these specified applications. This field of study can present multiple parameters correlated to the laser power and time – dielectric breakdown, surface roughness, surface temperature, and laser induced damage threshold to name a few.

Figure 1.1.2. A hand-held Nd:YAG laser.[5] (public domain)

In the area of military defense, lasers are used to detect and destroy specified targets of interest. Therefore, the synthesis and functionalizing of materials that can withstand laser degradation has become of vast interest. As seen in figure1.1.2, lasers

such as a Nd:YAG laser have become hand-held devices and are used in the line of duty. Currently, gas lasers such as a CO_2 laser require heavy and fragile components that consume so much space. Because of this structural difference, YAG lasers have become more popular. The advancements in technology have allowed the necessary components to be condensed, and the device has become a hand-held unit. A detailed overview of laser components and an explanation of why YAG lasers are used in laser interaction applications with composites are given in chapter 3.

1.2. Carbon Fiber Reinforced Multifunctional Composites

Fiber reinforced composites have a wide range of applications, such as, nautical automobile frame components[4], aerospace vehicles[6], and small airframe design apparatus.[7] The central goal of multifunctional fiber reinforced composites in these applications is to achieve high strength to weight ratios at a low cost. While multiple polymers have been tested in industry and research based composite applications, carbon fibers have been mostly pursued for its efficiency in reproducibility, simple production method, enhanced strength to weight ratio, and tensile strength. Typically, fiber reinforced composites are made in 3, 4, or 6-ply schemes to exploit these morphological and mechanical capabilities. Additionally, carbon fiber alignment has also been investigated and proven to have direction dependency of the mechanical properties. Tensile, compression, and elasticity strengths vary based on the alignment of the fibers. While there are numerous weave patterns in current use and being designed for future applications, the most common weave patterns used in composite based airframe designs

are 0°/90° and +/- 45°. Alternating these weave patterns give a better mechanical response as opposed to using one pattern style.[8-13]

In addition to the mechanical properties, more specifically, recent research efforts have been aimed at designing materials and composite layup schemes that can increase two or more properties (i.e., thermal, electrical, etc.). Recent composite designs are being altered to incorporate multiple reactions based on the composite's reaction to its surrounding environment. For example, the implementation of carbon nanotube sheets (or buckypaper) has been shown to increase composite's mechanical strength, thermal stability, and electromagnetic shielding capabilities [14-16]**.** While all of the composite fabrication techniques share similarities, the VARTM procedure is of interest because:

- it places the laminate under vacuum lowering chances of air pockets,
- high rate of uniform resin distribution,
- low cost tooling,
- the process does not require high heat or pressure, and
- it is a simple, one-shot process for large, complex parts

Recent trends in composite research include the development of structural materials with multiple functionalities, such as sensing and actuating.[17] Typically, an increase in functionality requires additional material phases to function within one system. The presence of excessive phases can result in deterioration of individual or overall properties of the system. True multi-functional materials must maintain all properties at or above the minimum operating limit, which can theoretically be achieved through volume fraction optimization. Figure 1.2.1 shows a Lockhead Martin F-22 fighter jet that has wings made from carbon fiber reinforced composites enclosed in metal

casings to improve the flight weight of the aircraft. .[9] Because of this feature, aircrafts become more maneuverable, or the structure can take on additional weight in other areas such as cargo, engine parts, and munitions.

Figure 1.2.1. Lockhead Martin F-22 Fighter Jet.[18] (public domain)

Multifunctional carbon fiber composites have become vital components in the development of defensive weaponry and aircraft designs and have even expanded into multiple areas of research. For instance, military soldiers have expressed concerns about new threats that they face while completing a missions using aerial vehicles comprised of fiber reinforced composites. In an effort to address these issues, defensive mechanisms are being integrated into the design of multifunctional carbon fiber composites. A review of carbon fiber composites is given in chapter 2.

1.3. Sol-gel Coating Applications and Techniques for Reinforcing Composites

In past research, reflection and absorption for specified wavelengths has been demonstrated by various materials on the micro and nanometer scale.[19] Thermal infrared radiation reflective property of the selected materials is mainly based on low emissivity. Typically, a low-emissive coating can reflect 85-95% of the thermal radiation while still allowing 60-65% transmittance of optical wavelengths.

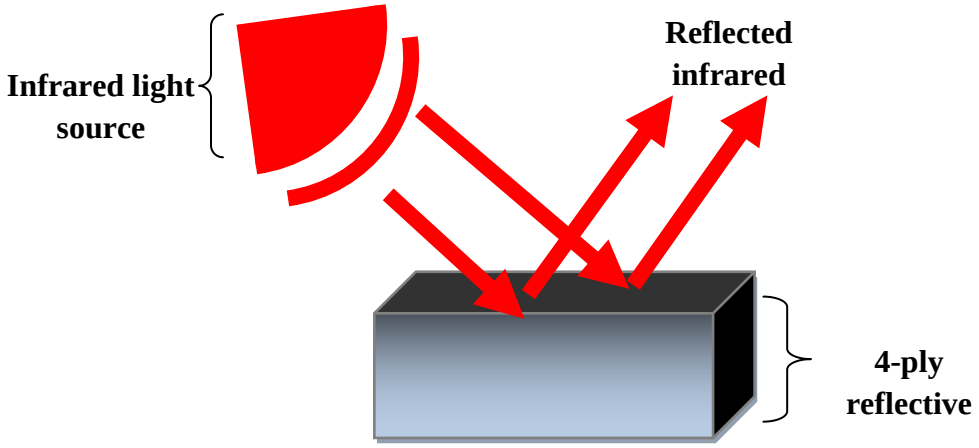

Figure 1.3.1. Infrared light from a monochromatic infrared light source being reflected off the surface of a 4-ply reflective composite.

A wide range of applications such as telecommunication system chips[20], window pane sensors for greenhouses[21], and junction layers for solar cells[3] have been developed from these material advancements. In relation to this proposed research, it has been demonstrated that chemically tailored oxides deposited on fiber surfaces can reflect in a desired range of wavelengths. The application of reflective sol-gels being incorporated into composites has been examined in previous research[22], but literature is limited to a selective amount of dopants being added to metal oxide sol-gel solutions.

Figure 1.3.1 gives an illustration of an infrared reflective composite design demonstrating the ability of a composite to reflect. Reflection capabilities are also a result of dopant concentration and morphology. For example, antimony (Sb) doped tin oxide (SnO_2), or (ATO), has been proven to have high conductivity, low resistivity, high transparency in the visible range, and thermal infrared reflective (TIR) properties.[23-30] Also, research has shown that the combination of metal oxide sol gels with ferromagnetic materials can increase the uniform coverage and the infrared reflectivity.[31-33]

1.4. Contributions to the Practice, Goals, and Objectives

1.4.1. Contributions to the Practice

Since the invention of the laser by Dr. Charles Townes and and Dr. Aurther Schawlow in 1958 at Bell Labs, physicists and engineers have been inquisitive on the possibilities of creating a laser weaponry. Within the past 10 years, scientists, several military branches, and the Department of Defense have collaborated to produce such a product in multiple research efforts. Collectively, the main objective was to design a laser that can focus high energy on a specified target and be used as a weapon against threats or attacks. From these efforts, such projects as the Airborne Laser Project (ABL) and the Advanced Tactical Laser Project (ATL) have been created. These projects mainly differ in target sensor range. While the ABL project was used to sense and destroy ballistics of high altitude, the ATL project was used as an accompaniment for ballistics of mid and low range altitude.

Because of this effort, the Air Force has expressed concern in designing coatings of high reflectivity to combat similar systems that may be used as threats to our environment. Particularly, recent efforts in reflective composite design have become of concern for protection against laser degradation to mid and low range ballistics frames containing fiber reinforced composites. This presented research serves as an effort to design a high reflective coating, capable of reflecting certain wavelengths and intensities and minimizing effects of strength to weight ratio. In addition, contribution to the practice involves composite-based coatings for unmanned aerial vehicles (UAVs) and their role in the front line of duty. Soldiers currently use these RC-controlled aerial vehicles to survey the land before they enter for possible traps, bombs, and attacks. Enemies of war have been aware of this precautious tactic, and have the capability of using handheld Nd-YAG lasers and other portable, target-locking systems to burn holes in the airframe. This causes the UAV to crash long before the mission is complete. Designing a coating that can prevent laser degradation yet add virtually negligible weight to the deployed airframe or munitions is of importance to the Air Force. The fabrication technique presented in this work demonstrates how tin oxide co-doped with antimony and cobalt oxide ATO(Co_2O_3) can be implemented into the design of carbon fiber-based airframes and munitions as a sol-gel coating and provide protection against thermal infrared damage at 1064 nm. While previous research has confirmed the mechanical and thermal properties of carbon fiber reinforced composites, no previous research has examined the thermal, mechanical and optical enhancements of a metal oxide sol-gel coating on carbon fibers. From this work, future applications including multiferroic

composites, fiber-reinforced munitions, and aerospace vehicle frames will benefit from the data provided from the in-depth investigation.

1.4.2. Goals and Objectives

Progress made by this research will satisfy the primary objective - to enhance carbon fiber composite-based aircraft capabilities to withstand infrared laser degradation. Optimization of the ATO(Co_2O_3) sol gel deposition process, doping concentration, and interaction with the carbon fiber surface will be defined for maximum optical and thermal performance. In an effort to efficiently examine the optical parameters and obtain sufficient data to satisfy the primary goal, the following objectives have been identified:

1. Investigate the optical effects of heat treatment on ATO sol-gel thin films.

   This is to reduce the error in data efficiency while using the chosen methods of characterization - FTIR, SEM-EDS, and Raman spectroscopy. This process was used to obtain baseline data of the sol-gel chemical composition and imaging and confirm with previously reported data.

2. Examine the optical effects of heat treatment on ATO(0.1%Co_2O_3).

   This step was also done to examine the sol-gel coating as a thin film to determine optimal heat treatment levels as well as maximum possible reflectivity. Fluctuation in optical parameters was observed at low doping levels of Co_2O_3.

3. Determine the angle-dependent reflectivity of the ATO(Co_2O_3) sol-gel coating on carbon fiber mats, and correlate the maximum reflectivity to the level of Co_2O_3 (0.2-0.5%).

   The data obtained for this objective will solidify the presented results confirming the primary objective has been completed.

Two sample preparation processes were used to accomplish the aforementioned goals. For the thin film analysis, 20 μL of the sol-gel solution was spin coated on silicon and carbon/silicon substrates. This sample setup was designed to compensate for the conformal surface of carbon fibers, yet it still allows characterization of the interaction of the sol-gel coating with a carbon surface. The second sample setup used 3-inch carbon fiber mats immersed in the sol-gel solution and heat treated at specified temperatures of 250 °C. This was done to examine the effects of the sol-gel coating on a carbon fiber mat on a microscale and macroscale.

1.5. Organization of the Dissertation

A brief overview of the relative characteristics of carbon fiber composites, infrared lasers, and sol-gel applications for this project are presented. Also, the discussion of the necessity of the data obtained and the goals and objectives of this research are discussed in this initial chapter.

Chapter 2 provides a theoretical background on lasers and laser radiation, followed by a discussion on the current state of the art for infrared laser applications. Additionally, as a discussion of reflectivity is given, its relevance to this research and the

propagation of light through oxide materials are presented. The theory and application of laser induced damage threshold experiments are discussed, and the selection of materials for this research are identified. Additionally, previous, public-accessed government programs involving defensive laser ablation are discussed, and this information is used to express the necessity of this research.

Chapter 3 discusses the previous research that is vital to the success of this research. Chapter 4 presents the results from ATO sol-gel coating of carbon fibers. Nanoscale investigations from chapter 2 and 3 are then compared to results on a macroscale.

In chapter 5, the structural and composition effects of Co_2O_3 as a dopant in ATO sol-gel thin films are examined from a material science perspective. The methodology of fabrication and quantitative testing parameters are discussed. Chapter 6 presents reflectance and absorbance measurements of ATO(Co_2O_3) sol-gel coated carbon fibers. It is shown that these parameters fluctuate at different dopant levels when varying wavelengths, angle dependency, and temperature.

Chapter 7 concludes the research effort, summarizing the results of the sol-gel coating and providing future directions of sol-gel coated fiber applications. Additionally, dialogue on the implementation of the oxide coatings in other optical-based oxide thin film applications is presented.

CHAPTER 2

LITERATURE REVIEW

2.1. Theory of Lasers

Optics is defined as the branch of physics which investigates the study of light and its behavior independently as well as its interactions with matter. Optics also involves the study of the instruments used to direct, focus, or manipulate light.[34] Light can be described as both a particle and a wave. When discussed as a particle, light is formed by atoms in a medium being energized to an excited state. Once these atoms start to lose energy, they descend back to their original state, emitting excess energy. While this excess energy can be released in the form of heat, it can also be seen in the form of photons, or what we perceive as light. When light is described as a wave, it can be described as an electromagnetic wave containing perpendicularly aligned electric and magnetic waves, which are also perpendicular to the wave's direction of travel. The equations in the following section have been further derived and referenced [34].

In 1923, Louis de Broglie discovered another vital relationship between energy and the speed of light. It was found that a constant value, known as the Planck's constant, could be used to represent the correlation of the momentum and wavelength of

a photon. If the frequency of a wave is known, it was shown that the energy could be calculated from this equation:

$$E = h * \nu = h * (\frac{c}{\lambda})$$

where E is energy, h is planck's constant, v is frequency, c is the speed of light ($3*10^8$), and λ is the wavelength. Because of these founding equations, the following conclusions were also shown:

- As frequency increases, the wavelength decreases
- As frequency increases, the photon energy increases
- As the wavelength decreases, the photon energy increases

Longer wavelengths produce lower energies, while shorter wavelengths produce higher energies.

The laser beam strength, or output power, can be determined by the average energy states of the conduction and valence bands divided by the difference in time ($\Delta T = T_2-T_1$) the beam is emitted:

$$P_{out} = \frac{\Delta E}{\Delta T}$$

The unit of measurement for power is watts, which are joules per second. From these emitted photons, other atoms are accelerated into excited states. This chain reaction continues to take place until there are (theoretically) no more atoms in the ground state. The word "laser" comes from the acronym LASER, meaning light amplification of stimulated emission from radiation. This is done on the molecular level by two types of emissions, spontaneous and stimulated. In spontaneous emission, a natural occurrence of atoms dropping to their lowest possible state is observed. In stimulated emission,

specified light waves of photon energies are used to illuminate and excite atoms to a higher energy state. The atoms begin oscillating at the incident light wave's frequency. This oscillation then in turn amplifies the original light wave. The ratio of atoms in different energy states (N_2/N_1) is exponentially proportional to the difference in energy states (E_2-E_1) divided by the product of Boltzmann's constant, k_B and the temperature, T:

$$\frac{N_2}{N_1} = \exp[-\frac{E_2 - E_1}{k_B T}]$$

This radiation of stimulated emission is possible by the regeneration of photons, or light. The wavelength, λ, of light is defined as the distance between two peaks of energy in a light wave. The wavelength of this light is determined by the difference in energy states of the conduction and valence bands ($\Delta E = E_2$-E_1):

$$\lambda_0 = \frac{1.2398}{\Delta E}$$

The wavelength of a laser source is dependent on the material, the optical system, and the energizing process. Also, the spectra of wavelengths inside a laser beam determine its classification. A monochromatic laser is single-colored and emits one specified wavelength, while a multiline laser contains 2 or more wavelengths in its beam. The frequency, ν, is defined as the number of peaks per second (Hz). The correlation of frequency and wavelength is governed by the speed of light, c:

$$\nu * \lambda = c$$

From these governing principles, the ideas and invention of masers (microwave amplification by stimulated emission of radiation) was invented in 1951 by Townes and Schawlow. The motivation behind the invention was the idea that a stable frequency source can be produced by utilizing a transition between the energy levels of an atom or a

molecule. This invention was used in applications such as low-noise amplifiers for high-sensitivity radar radio telescope. Masers were the predecessors to lasers, which now rank as the highest-performance devices for frequency standards.[2] The first laser was invented in 1960 by Maiman.[3-4] In his development, he used a ruby as the laser medium and discussed the fluorescent relaxation processes, the ground-state population changes due to optical excitation, and the detection of optical absorption between two excited states. From his efforts, many other research groups designed lasers of different medium materials and produced lasers of both pulse and CW.[5-7]

Lasers can operate in two modes, pulsed or continuous wave (CW). The main difference between these modes is the maximum possible average power provided to the sample or specimen of interest. For instance, Nd:YAG lasers can operate at 40 to 60 watts in pulse mode. However, the same laser can only operate at ~10 watts in CW mode. The reason for this effect is because pulsed lasers have the capability to cool down in between exposure. Depending on the rate of pulse, pulse lasers can easily be mistaken for CW mode lasers.

There are various groups of lasers, such as gas and liquid lasers, solid-state lasers, and semiconductor lasers. These lasers are grouped by the materials used in the medium and their process of producing a laser.

2.2. Infrared Radiation

From derivation of Maxwell's equations, the function of an electromagnetic wave (i.e., light) can be defined as:

$$E_x = e^{i\omega(t-\left(\frac{nz}{c}\right))}e^{-\omega kz/c},$$

where ω is the angular frequency, t is the time interval, n is the refractive index, c is the speed of light, and z is the wave impedance. The squared wave impedance of a medium is proportional to the dielectric permittivity divided by its magnetic permeability:

$$\frac{\mu}{\epsilon} = z^2 \rightarrow \sqrt{\frac{\mu}{\epsilon}} = z.$$

The function E_x states that an electromagnetic wave can be transmitted through a material with an associated electromagnetic field of period nz/c and with an exponential absorption of $e^{-\omega kz/c}$.[8] Figure 2.2.1 shows the interaction of an electromagnetic wave with a surface.

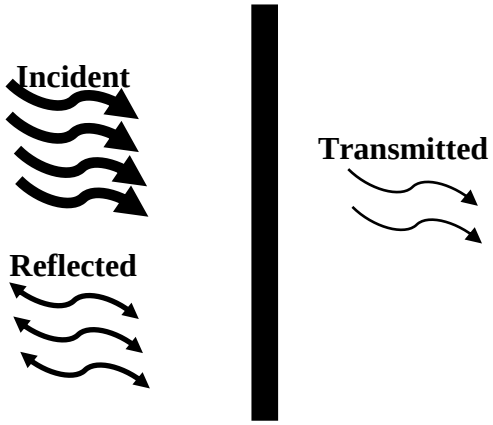

Figure 2.2.1. Reflected and transmitted waves from an incident wave at a surface.

From figure 2.2.1, it is seen that the field vectors for each set of waves are continuous. Because $E_y/H_x = z$, $E'_y/H'_x = z'$, and $E''_y/H''_x = -z$, Poynting's vector law is then proven and the propagated energy in the wave is

$$(\frac{\varepsilon}{\mu})^{1/2} = n_1 E^2$$

The proportion of reflected energy is defined by:

$$R = (n_0 - n_1)^2,$$

and the transmitted energy is equated by:

$$T = \frac{4n_0 n_1}{(n_0 - n_1)^2}$$

2.3. Theory of Thermal Infrared Reflectivity

The design of an infrared reflective coating is governed by multiple theorems and models. In such, two key phenomenon have been identified in the fabrication process. First, the heat treatment temperature (also known as the sintering or annealing temperature) alters the crystal lattice alignment as well as the atom placement. This has been proven in literature through numerous experiments. Secondly, the charge carrier density and thermal emissivity are changed by way of the applied heat treatment. Previous experimental results show the optical and thermal affects of doping concentration. In understanding the complex atomic interactions that occur at the surface level, a discussion on the governing equations and models is given.

In everyday life, we see the exchange between the color of a surface and the heat it emits to its surrounding. This is commonly seen in items such as ignited fire wood, light bulbs, or stove heating elements. This observation shows two effects of thermal radiation based on its appearance and how it affects its surroundings. The amount of

emitted radiation is directly proportional to an object's temperature, hence the explanation to the examples given.

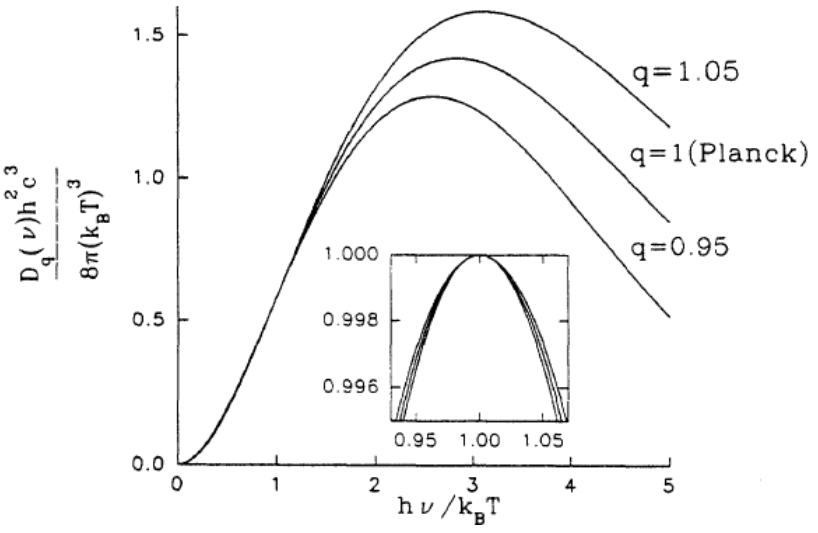

Figure 2.3.1. Blackbody photon energy with extensive (q = 1) and nonextensive (q = 0.95 and 1.05) statistical mechanics.[35]

Blackbody radiation is used to describe the electromagnetic radiation within or surrounding an object in thermal equilibrium with its surroundings. The foundation of the radiation laws are derived on the assumption that the object under observation is in a surrounding environment at a blackbody temperature. Planck's Law of Radiation defines the intensity of emitted radiation from a unit surface area as a function of wavelength for a fixed temperature:

$$E_{(\lambda,T)} = \left(\frac{hc}{\lambda^5}\right)\left(\frac{1}{e^{\left(\frac{hc}{\lambda kT}\right)} - 1}\right),$$

where h = $6.626*10^{-27}$ erg*sec, k = $1.38*10^{-16}$ erg/K, and c = $3*10^{8}$ m/sec. As shown in figure 2.3.1, as the temperature increases, the peak shifts toward shorter wavelengths.

In an effort to describe these peak shifts in Planck's Law, Wein's Law and the Stefan-Boltzmann Law are derived. Wein's Law states that the peak wavelengths in the distribution of thermal radiation can be calculated by $3*10^{7}$ divided by the temperature, T:

$$\lambda_{max} = \frac{3 * 10^7}{T}$$

while the Stefan-Boltzman Law gives the blackbody energy at all observed wavelengths:

$$E = \sigma T^4$$

Two types of reflection can occur. Specular reflection occurs from radiation on smooth surfaces, while diffuse reflection occurs from radiation on rough surfaces. It can be shown through reflectance experiments that most materials contain both a specular component and a diffusion component. The specular component of a material is wider when reflection is given from a smoother surface at a specific angle. The diffusive component takes place at a wider range of angles, which makes it more common in reflective measurements. However, some systems calculate and correct measurements, removing or separating the specular component out of the reading. This is performed to better evaluate the reflectance components independently without merging the two components together, which may then cause discrepancy where an increase in reflectance is seen.

When discussing interactions of light with matter, there are three distinctive classes of objects:

1. transparent – objects capable of transmitting light
2. opaque – objects that absorb light
3. reflective – objects that reflect light

While these classifications are used, it is known that there is no one true material to any group, as all materials transmit, absorb and reflect some percentage of light. However, materials are labeled as such based upon the dominating effect of radiating light in a specified spectrum. For instance, tin oxide is a well known material that is transmittal in the visible range, absorbent in the ultraviolent (or UV) range, and reflective in the infrared (or IR) range.[28, 36-39]

The basic law of reflection states that the incident angle is equal to the angle of reflection. It is also known from the derivation of Fresnel's equations of reflectivity that reflectivity coefficients can be calculated from the transmission coefficients:

$$T = 1 - r, so\ r = 1 - T$$

Therefore, in the collected transmission data, reflectivity components can be calculated. Reflectivity is defined as a

of radiant flux reflected divided by the incident radiant flux:

$$\rho = \frac{\Phi_r}{\Phi_i}$$

whereas spectral reflectance factor (R), or reflectance in relation to a specified wavelength, is defined as the ratio of spectral flux reflected from an object (Φ_s)to the spectral flux reflected from a perfect diffuse (lambertian) reflector (Φ_o):

$$R = \Phi_s/\Phi_o$$

We then take the preceding definition of reflectivity to derive the Stefan-Boltzmann Law. In calculating all reflectivity at a specific wavelength, it is shown that

$$I = \sigma T^4 = \int_0^\infty R_\lambda d_\lambda, \text{ where } R_\lambda = \left(\frac{c}{4}\right)\left(\frac{8\pi}{\lambda^4}\right)\left(\frac{\frac{hc}{\lambda}}{e^{\frac{hc}{\lambda k_B T}}-1}\right)$$

It is seen that:

$$I = \int_0^\infty \left(\frac{8\pi c}{4}\right)\left(\frac{hc}{\lambda^5}\right)\left(\frac{1}{e^{hc/\lambda k_B T)}-1}\right) d\lambda$$

Substituting x for $\frac{hc}{\lambda k_B T}$, λ then becomes $\left(\frac{1}{x}\right)\left(\frac{hc}{\lambda k_B T}\right)$, and dλ goes to $-\left(\frac{dx}{x^2}\right)\left(\frac{hc}{k_B T}\right)$.

So:

$$I = \left(\frac{8\pi c}{4}\right)\left(\frac{k_B T^4}{hc^3}\right)\int_0^\infty \left(\frac{x^3 dx}{e^x - 1}\right) = \left(\frac{8\pi c}{4}\right)\left(\frac{k_B T^4}{hc^3}\right)\left(\frac{(\pi^4)}{15}\right)$$

It is seen now that:

$$\sigma = \left(\frac{2\pi^5\left(k_B{}^4\right)}{15c^2h^3}\right), \text{ and, therefore } I = \sigma T^4$$

In essence, the Wein's Law explains the peak shifts in wavelengths, while Stefan-Boltzmann Law explains the rate of growth in temperature. The Stefan-Boltzmann Law also shows that the thermal emissivity of a material affects its infrared reflectivity.

2.4. Laser-induced Damage Threshold Theory

The purpose of laser induced damage threshold experiments are to investigate the surface roughness, dielectric breakdown, and surface temperature effects of a specified material having undergone direct radiation from a radiation source, typically a medium or

high power laser. This is of interest to the Air Force Research Laboratories (AFRL) for current undisclosed military applications. In general, the breakdown time in correlation with the applied laser power in both instances of pulse count and duration time is of interest. This information is to assist in the design of a thermal infrared reflective coating for carbon fiber composites. Furthermore, the information obtained from this report will contribute to the body of knowledge for such materials in multiple applications such as optoelectronics, transparent conductive oxides for solar cells, and light emitting diodes. Laser-induced damage threshold (LIDT) is defined as the highest fluence for which no damage has been observed.

ATO is transparent in the visible spectra, absorbing in the UV spectra, and reflective in the near infrared range (0.7 – 1.2 μm). The increase in heat treatment temperatures will decrease defects and dislocations in the sol-gel coating's stoichiometry. A Nd:YAG laser of 1064 nm (1.064 μm) pulsing at 10 ns with a beam width of 100 μm will show that the LIDT will vary around 23 J/cm^2. The resin used to make the composite is predicted to be evaporated by the laser and to not alter the LIDT. Heat treatments applied to the ATO(Co) sol-gel coatings alter their crystallography and optical parameters.

2.5. Sol-gel Fabrication

The sol-gel method consists of two commonly used methods, the all-alkoxide and alkoxide-salt methods, as well as a few unconventional approaches.[3, 20, 40, 41] However, all processes result in a homogeneous mixture of desired oxide components

that are made at low temperature and result in high quality films. Also, the oxide precursors are soluble in organic solvents and easily convertible to the desired oxide material by way of a chemical, thermal or oxidative-based reaction. In the all-alkoxide method, a metal material is paired with an alkyl group, and the valence state of the solution identifies the ionization of the metal. These metal alkoxides are hydrolyzed to produce the specified oxide. The chemical reaction is denoted in empirical formula notation as:

$$M(OR)_x + xH_2O \rightarrow M(OH)_x + xROH$$

$$2M(OH)_x \rightarrow M_2O_x + xH_2O$$

M is the metal, R is the alkyl group, and x is the valence state of the metal. ROH is an aliphatic alcohol that can be removed from the solution by way of drying at temperatures at or above room temperature.

More alkoxides in the solution present complexity into the sol-gel formation. In certain hydrolysis with alkoxides, such as silicon and phosphorous, the hydrolysis rate is faster than common hydrolysis rates of other alkoxides. This leads to possible non-homogeneity. In order to slow this process, the alkoxide is produced in a rate-slowing solvent before being exposed to atmospheric pressure. Adding this step into the process could slow down gelation of a solution to days or even weeks before complete formation. The second most commonly used sol-gel fabrication method is the alkoxide method. This approach allows solid metals of low solubility to be formed into sol-gel thin films.

Elements, such as Group I and Group II, present difficulty when trying to obtain pure forms to prepare under complex preparation procedures.

So, metal salts are used in a similar chemical reaction. However, the formation of the specified metal oxide is dependent on thermal or oxidative decomposition. The overall process involves using metal salts in alcohol or water solutions to alkoxide mixtures for hydrolysis. Based on the chemical reactions, this causes uniform dispersion. If the reaction rate is still too fast, previously mentioned techniques for alkoxide solutions can also be used in this approach.

2.6. Characterization Methods

2.6.1. Surface Morphology Imaging – Scanning Electron Microscopy

Scanning electron microscopy (SEM) was used to image the surface of the sol-gel thin films and coatings on carbon fiber surfaces. Figure 2.6.1 shows a Hitachi S800 scanning electron microscope. The fundamentals of this imaging technique involves the use of a high powered electron beam of up to 25 kV produced by a thermionic field emission gun/power source. As the beam travels downward towards the sample, condenser lenses place a magnetic force upon the beam to uniformly focus its energy in a downward direction. Next, an objective lens is used to focus the beam in a smaller dimension. As the electrons strike the surface of the sample, secondary electrons are emitted from the sample surface. As these secondary electrons are emitted, a everhart-thornley detector collects some of the electrons and configures it to an electronic image.

Figure 2.6.1. Hitachi S800 scanning electron microscope.

The type of material that is being examined emits specified energy levels of electrons. A three dimensional surface can be seen by the level of energy being collected by the everhart-thornley detector. Since the sample is placed in a vacuum environment, normal scanning electron microscopy standards require that the sample is non-liquid and conductive. For materials such as polymers, the sample surface can be electrically charged by the electron beam. To correct this issue, a lower voltage is used, preferably 5-15 kV. While this can allow minimal imaging, high resolution and high magnification parameters cannot be met on non-conductive surfaces. For this research, the thin films of metal oxide sol-gels were conductive, and were examined at high resolution parameters. Because of this, high quality imaging of the surface quality, mainly for surface roughness

and uniform coverage, was observed. For imaging of the sol-gel coated carbon fibers, 20-25 kV was used to compensate the charging effect on the carbon fiber surfaces, as electrons often penetrated the sol-gel surface.

2.6.2. Composition Detection - Energy Dispersive Spectroscopy

Energy dispersion is a technique that is performed with the scanning electron microscope. While the electron beam causes secondary electrons to emit from the surface, characteristic x-ray electrons are also emitted.

Figure 2.6.2. EDAX detector for energy dispersive spectroscopy.

An EDAX detector is used to collect the x-ray electrons and work coinciding with manufactured software to identify the specific elements present in the sample. Figure 2.6.2 shows the EDAX detector connected to the Hitachi S800 SEM. A two dimensional

plot is used to show the type of material and shell type of the electron energy versus the number of counts from that material. The shell type can be identified by the known amount of energy required to break the electron away from a specified level of orbit. This information is beneficial to those in the materials science, chemistry, or physics field, where the examination of electron interaction is vital.

2.6.3. Optical Response – Raman Spectroscopy and Fourier Transform Infrared Spectroscopy

Raman spectroscopy is used to investigate the elastic and inelastic scattering of incident infrared light from the crystal lattice of atomic structures. This characterization method can be used to identify chemical bonds of known materials at specified wavelengths of reflection and wavenumber shifting. Once the incident laser is absorbed at a specific wavelength, a photon is emitted at a longer coinciding wavelength. The chemical bonding is then verified with the decay of excitation states relevant to that material. There are two common forms of plots shown from Raman spectroscopy.

Generally, the plotting of Raman spectroscopy data shows the wavenumber of incident infrared light versus the percentage of reflectivity. However, depending on the application and focus of research, the data can be plotted to show the loss (anti-stokes scattering) or gain (stokes scattering) of energy. Figure 2.6.3 shows the Horiba HR800 Raman spectrometer. Similar to Raman spectroscopy, fourier transform infrared spectroscopy (FT-IR) is also a technique founded upon the study of radiated light interaction with materials. Infrared photons cause chemical bonds to stretch and bend.

Characteristic frequencies are based upon the transition between quantized vibrational energy states. Figure 2.6.4 shows an FT-IR.

Figure 2.6.3. The Horiba HR800 Raman Spectrometer.

Figure 2.6.4. Nicholson 6700 FT-IR system.

FT-IR can cover the near, mid, and far infrared ranges (10-14000 cm^{-1}). A typical FT-IR system contains a Nd:Yag laser of 1.064 μm wavelength. Inside, a Michelson interferometer set up is used to reflect the light through or off of the sample and detect the vibrations of the crystal lattice. There are four modes of FT-IR: 1) transmission, 2) specular reflection, 3) diffuse reflection, and 4) attenuated total reflection (ATR). For our samples, ATR was chosen as our characterization method. This was selected because the samples were tested with little or no modifications for sample preparation.

Also, in ATR modes, the infrared light is allowed to pass through the sample multiple times before being collected by the detector. The only setback from ATR is the data may not be accurate if the sample is not in close contact with the background crystal. However, to compensate for this possible error, our testing was verified through multiple runs. In plotting FT-IR data, percent reflectance versus the wavenumber is commonly used. From this, chemical bonds at specific wavelengths can be identified by drops and slopes in the percent reflectance. Chemical bonds are then identified with previous plots of FT-IR data conducted on similar material.

2.6.4. Hemispherical Integrated Reflectance - Spectroradiometer Spectroscopy

This unique reflectance test is done with a spectroradiometric measurement system. Figures 2.6.5 shows the hemispherical integrated reflectance spectroscopy system, while figure 2.6.6 shows the schematic drawing of a Gooch and Housego OL 740-70 integrating sphere reflectance attachment. Figure 2.6.7 provides a look at the circuitry inside the infrared light source. In detail, the sample is placed at a flat opening

of a sphere. Inside this sphere is 99.999% reflective material that reflects the light throughout the sphere and onto the sample. A detector, also located inside this sphere, is placed at a 10 degree angle referenced to the sample.

Figure 2.6.5. Gooch and Housego OL Series 750 Spectroradiometric Measurement System with an OL 740-70 integrating sphere reflectance attachment.

The detector then examines how the reflectance changes once a sample is used to close the sphere. Also, during our testing, a "blackout" cloth was placed over the entire system to eliminate or minimize random light interference. For our measurements, 99.9% reflective spectralon SR99 was used as the reference reflectance material. This is a calibration standard for reflective measurements. An additional attachment could also remove the specular component of reflectivity from the measurements. However, for our sample testing and application purposes, the specular component was included. This was done to simplify testing methods and calculation, as total reflectivity is used when calculating the absorption. With this system, measurements can be taken from 200 nm to

2.5 µm wavelengths, and sample sizes can range from 1 inch in diameter to 2 x 4 inches. However, for our testing in the thermal infrared range, a gold coated integrating sphere attachment enables 10-degree hemispherical reflectance measurements to be made from 2 to 15 um wavelengths.

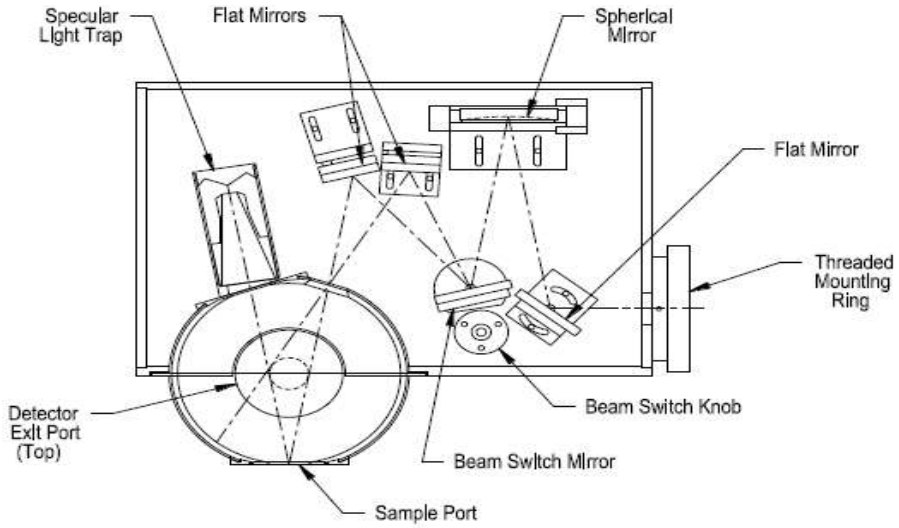

Figure 2.6.6. Schematic drawing of a Gooch and Housego OL 740-70 integrating sphere reflectance attachment.

Figure 2.6.7. Hemispherical Spectrometer infrared bulb source.

2.6.5. Angular-dependent Bi-static Transmittance – Enhanced FT-IR Spectroscopy

The bi-static transmittance system is a patented system by Dennis Goldstein, Ph.D. (U.S. Patent Number 6,618,145) that involves a bio-rad FTS 6000 FT-IR system, a rotating detector, and standard optics mounting equipment. In this setup, measurement testing ranges from 0.7 to 10 μm. While the application purposes relevant to this research required a bi-static setup, the rotating detector allows monostatic setup capability. Figure 2.6.8 shows the bi-static transmittance setup. In the accompanied software, steps between each μm wavelength and wavelength range are specified. The Nd:Yag laser in the FT-IR system is used as the laser source.

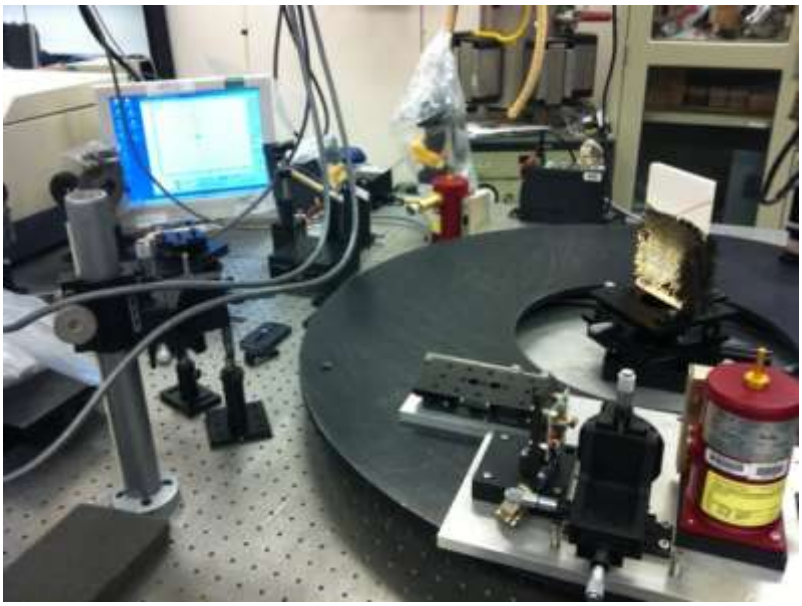

Figure 2.6.8. Bi-static fourier transform infrared spectrometer setup.

Screens are placed in front of the FT-IR source to compensate for attenuation. The detector has a rotation range of 0 – 100 degrees. Because of the rotation of the detector,

the sample size requirement is 3 inches in height and 3 – 5 inches in width. This is because the beam diameter stretches from circular to an oval shape when the detector rotates ±45 degrees. The data is collected by the software and exported into excel file text data. Similar to FT-IR spectroscopy, both transmittance and reflectance data are plotted versus the wavelength.

2.7. COMSOL Simulations

In an effort to characterize a predict model for the composites, a finite element analysis simulation software, COMSOL, was utilized. The finite element analysis simulation models were modified from examples listed in the software documentation. [49] The components in the original module are contained in a chamber with temperature-controlled walls with a set point of 400 K. The result is results in a closed cavity allowing one to control the surrounding environment. Furthermore, the model assumes that this physical system is dominated by radiation and convection cooling. The convective cooling of the oxide layer and sensor to the gas (at 400 K) is modeled using a heat transfer coefficient, h (in this example set to 20 W/(m^2·K)). The problem is governed by the heat equation, given below together with its boundary conditions:

$$\rho C\left(\frac{\partial T}{\partial t}\right) + \nabla * (-\kappa \nabla T) = Q$$

$$-n * (-\kappa \nabla T) = h(T(inf) - T) + \left(\frac{\boldsymbol{\varepsilon}}{\mathbf{1} - \boldsymbol{\varepsilon}}\right)(\boldsymbol{J}(\boldsymbol{o}) - \boldsymbol{\sigma T^4})$$

where ρ is the density; k denotes the thermal conductivity; Q represents the volume heat source; n is the surface normal vector; $T_{(\text{inf})}$ equals the temperature of the convection cooling gas; ε denotes the surface emissivity; J_0 is the expression for surface radiosity and κ is the Stefan-Boltzmann constant.

CHAPTER 3

BACKGROUND

3.1. Metal Oxide Coatings for Carbon Fiber Composites

The interaction of lasers with carbon fiber composites are of vital interest for multiple military applications. Initial research on electromagnetic interference (EMI) shielding incorporated heavy metal sheets into the body frames of aerial vehicles and missiles. As mentioned previously, carbon fibers were implemented into aerial vehicle and missile design because of their high strength to weight ratio, low density, and electrical conductivity. Because of new applications and heavier cargo, a lighter frame increases the flight time and reduces the amount of required power for takeoff and flight stability. Also, as new optical threats emerged decreasing successful mission efforts, advanced techniques were developed to counteract these methods of infiltration. From this, metal oxide coated carbon fibers were used in replacement of the heavier EMI metal frames.[42-47] The basis of the implementation of infrared reflective coatings is to reflect infrared light and uniformly distribute the heat across a carbon fiber composite surface. Another common application is microwave absorbing coatings for electromagnetic interference (EMI) shielding. Specific metal oxides are selected for these applications because of their absorption in the UV range and high reflectivity in the

near and mid infrared ranges. In the case of microwave EMI shielding, transmission and reflection coefficients through a coaxial system is measured and compared in decibels. [42-47] Higher reflection and lower transmission is desirable.

For infrared reflectivity, metal oxide coatings for applications such as solar windows and laser lenses were incorporated into the design of carbon fiber composite systems. The lower resistivity for the thicker film indicated a change in the microstructure, such as larger grain size and/or different properties at the grain boundaries. At wavelengths up to those where the reflectance increases strongly, the theory for ionized impurity scattering and the Drude theory are equally successful in reproducing the experimental data. However, at longer wavelengths, the Drude theory is superior. This is because the infrared reflectance basically depends on the DC resistivity, and since the measured $\rho(dc)$ was used as an input parameter in the Drude calculations, a good agreement is, in fact, expected. In the case of ionized impurity scattering, however, the resistivity in the infrared region was obtained as a result from the calculations, and it turns out that $\rho^{IIS}(\omega)$ is lower than the measured $\rho(dc)$ for all investigated films. Many of these metal oxides were tested for their dielectric breakdown and laser induced damage threshold.

3.2. Metal Oxide Coating Deposition Methods

Metal oxides can be deposited in various techniques, such as electroplating, chemical vapor deposition, electron beam evaporation, and dip coating [26, 31, 48-54]. However, control over the thickness and uniform surface coverage can only be achieved

with some percent error or difference, depending on the surface area size. In the majority of the previously mentioned deposition techniques, the substrate is usually heated or given a potential or charge difference to promote a successful uniform deposition. As discussed later in this chapter, in the case of cobalt, a heat substrate usually gives a smoother surface for deposition. Therefore, cobalt oxide exhibits better magnetic properties, such as coercivity, when deposited on a smoother surface. Also, a post annealing and heat treatment is given to most deposited metal oxides to: 1) assist in providing uniform coverage of the deposited material, 2) remove low concentrations of surface contaminants, and 3) further enhance the electrical, magnetic, and/or optical properties.

3.2.1. Electrochemical – Nanoparticle/Sol-gel Coating

Sol-gel coatings are the most commonly used in fiber coating techniques. Sol-gel solutions are typically deposited by method of immersion or dip coating. Also, like electroplating solutions, sol-gel fabrication allows complex materials to be added in controlled doping levels, which is very cost efficient when compared to other deposition techniques like CVD or sputtering. In both electroplating and immersion processes, after the sol-gel deposition, the acid or glycol used in the hydrosol solution is reacted with the nitrate or acetate through the chemical reaction process. Next, the annealing process is performed to activate chemical reactions in the coating solution. Since carbon fibers have high thermal stability, reaching towards 2000 °C (depending on which polymer is used to reinforce the carbon), it can easily withstand required annealing and heat treatment temperatures. This causes the acid to evaporate and create a byproduct residual

resulting in the uniform dispersion of the desired material on the fiber surface. Resulting dispersion can be verified via the combination of scanning electron microscopy (SEM) and energy dispersive x-ray spectroscopy (EDS).

Recent research initiatives have implemented nanoparticles into fiber reinforced composite systems. This is done by dispersing nanoparticles in sol-gel solutions. When not in bulk dry powder form, most oxide nanoparticles are developed and can be transported in a water-based solution. Uniform dispersion of the nanoparticles into a sol-gel solution is often done by ultrasonic dispersion. Other methods include magnetic stirring and chemical reaction-based dispersion.

3.2.2. Methods of Fiber Composite Coating Fabrication Techniques

Cobalt oxide sol-gels are usually formed by beginning with cobalt acetate (base/salt) in an acid solution. Drying temperatures are as low as 90 °C are used prior to annealing, and heat treatment temperatures range from 300-500 °C. While this is known, the previously mentioned materials can be deposited in various methods, such as electron beam evaporation, sputtering, and atomic layer deposition. However, there are various disadvantages that coincide with the advantages of using these deposition methods, as shown in table 3.2.1.

Acetone is typically used to strip industrial-standard carbon fibers of any post-manufacturing coatings that may be present and to clean the fibers for higher chemical reaction rates. Because of this, some type of acidic solution is used to promote better adhesion at the carbon surface. For instance, for electroplating oxalic acid is used to sensitize the carbon fibers, presenting more negatively charged ions at the carbon fiber

surface, thus promoting a higher quality of deposition. For immersion, ammonia (HNO_3) is used to introduce various functional groups, such as CO, OH, and COOH, at the carbon fiber surface. It has been shown that the hydrosol solutions make better bonds at the surface if this step is included.

Table 3.2.1. Advantages and disadvantages of currently used fiber coating techniques.

	Advantages	**Disadvantages**
Radio Frequency (RF) Sputtering	Uniform coating coverage (step coverage) Room and low temperature deposition conditions	Requires high voltage and current conditions High cost for specified doped targets
Atomic Layer Deposition	Deep trench deposition capability Angstrom level coating control	Not cost efficient No capability to incorporate ferromagnetic particles at low percentages
Electron Beam Evaporation	Thick coating coverage Metal and oxide deposition capabilities	Requires high voltage and current conditions Unstable conditions for oxides
Powder Coating	Wide range of oxide materials Allows ferromagnetic particle incorporation (pre-coating fabrication)	Does not provide a stable, uniform coating suitable for large-scale composites
Dip Coating (or Immersion)	Wide range of oxide materials Allows ferromagnetic particle and other sol-gel incorporation (pre-coating fabrication)	Inconsistency in thickness across the sample surface

Coating carbon fibers can be done by dip coating or immersion procedures. Dip coating allows for sol-gel thickness control by optimizing the dipping rate of the sample. In such cases where the thickness cannot be simply measured by profilometer techniques, it can be calculated based on the rate of deposition, the type of sample, and cross-

sectional area of deposition. In the electrochemical approach, fibers are immersed in the sol-gel solution, depending solely on the surface chemistry of the sample and sol-gel interaction to uniformly deposit a sol-gel coating.

The selected metal oxide sol gels have the ability to have the phase and/or band gap to be altered by the deposition procedure and heat treatment times and temperatures. This can have an adverse affect, as the mechanical properties of carbon fibers tend to degrade at temperatures above 400 °C. However, for instance, previous research reports that optimal crystallinity of TiO_2 is reached at 400-450 °C, while SnO_2 at 450-550 °C. Therefore, an optimal temperature is to be examined for maximum crystallinity in sol gel deposition with minimal carbon fiber mechanical degradation. While previous research has confirmed the mechanical and thermal properties of carbon fiber reinforced composites, no previous research has examined the thermal, mechanical and optical enhancements of metal oxide sol-gel coated carbon fibers.

3.3. Selection of Materials for Application

In the materials selection process, it was advantageous to be mindful of the currently used procedures used to make carbon fiber reinforced composites. In doing so, research on the possible fabrication techniques were reviewed and taken into consideration during the selection process. From these pioneering research advancements, other techniques have been developed such as compression, resin transfer molding (RTM), and, in particular, vacuum-assisted resin transfer molding (VARTM). As mentioned earlier, composites have a wide range of applications, ranging from aircraft

frame components[9], nautical automobile frame components[55], and aerospace vehicles.[4] While all of the composite fabrication techniques share similarities, the VARTM procedure is of interest because: (1) it places the laminate under vacuum lowering chances of air pockets; (2) it has a high rate of uniform resin distribution; (3) it has a low cost in tooling expenses; (4) the process does not require high heat or pressure, and (5) it is a simple, one-shot process for large, complex parts. Figure 3.3.1 shows a 3 x 5 inch carbon fiber composite fabricated by the VARTM method.

Figure 3.3.1. 4-ply carbon fiber composite.

From the evaluation of the commonly used technique to create carbon fiber composites, it was decided to use the sol-gel solution/precursor immersion process as the preferred deposition method. Selecting the sol-gel deposition gives multiple advantages that can easily be used for deposition purposes as well as implementation into the VARTM process. Also, from the conducted literature search, there is limited research

that has examined thermal and optical parameters of metal oxide sol-gel coatings specifically for infrared reflectivity on carbon fibers.

Oxides such as niobium, chromium, copper, titanium, and tin exhibit transparency in the visible range, absorption in the UV spectra, and reflectivity in the infrared range. Table 3.3.1 lists some parameters for commonly used oxides for infrared reflective coatings. It is the recombination of the ions in the crystal lattice with oxygen charge carriers that causes this phenomenon. Also, in perspective of the deposition method, the grain boundary size can be altered by applying heat at minimal temperatures for specified times. It is from this characteristic that the reflectivity, transmittance, or absorption of these oxides can be increased. Applications such as medium and high power laser lenses and solar reflecting window panes take advantage of these intrinsic properties. Many metal oxide sol-gel solutions such as tin oxide (SnO_2), titanium dioxide (TiO_2), chromium oxide (Cr_2O_3), and aluminum oxide (Al_2O_3). Sb-doped SnO_2 (ATO) have been proven to have high conductivity, low resistivity, high transparency in the visible range, and thermal infrared reflective (TIR) properties.[23, 25, 56-61]

In the transparent conductive oxide (TCO) research, many oxides, both simple and complex, are being produced in an effort to modify and control certain application-dependent properties. These properties may range from visible transparency, infrared reflectivity, and electrical conductivity (both AC and DC) to thermal conductivity and dielectric breakdown limits. Thermal collectors are a common application for transparent conductive oxides. The success of these materials in this application specifically is derived in the capability of absorbing solar light at specified wavelengths. In order to modify and control the selectivity of the absorbed spectrum, TCO's are being combined

with other elements such as fluorine (F), chromium (Cr), gallium (Ga), and molybdenum (Mo).

Table 3.3.1. Comparison of electrochromic materials.

	Sb-doped SnO_2	**Cr_2O_3 (undoped)**	**TiO_2 (undoped)**
Optimal Annealing Temperature (K)	723	873	673
Band Gap Energy (eV)	~3.6	~3.4	3.0 – 3.2
Reflectivity Spectral Range (nm)	620 – 640	2500 – 2600	388 – 413
Heat Treatment Range	450 – 550	350 – 400	400 – 450
Beneficial Parameters	Mid and far-range infrared reflectivity, oxidative resistant, band gap controlled by heat treatment and doping level.	2435 K melting temperature, oxidative resistant, mid-range infrared reflectivity	Near and mid-range infrared reflectivity, band gap controlled by heat treatment
Applications	Solar cell layers[62], optoelectronics [63, 64]]	Thermal coatings [65], solar energy collectors[66]	Optical and electronic devices[67]

A typical transmission range where a TCO performs efficiently is 0.4-15 μm. This is because, for shorter wavelengths, the transmission is dependent to the electron-interband transition. For longer wavelengths, a higher amount of light is reflected due to the plasma edge of the materials. In the visible spectrum, indium oxide is among the most commonly used materials in solar applications. Indium oxide has been used as a dopant to SnO_2 in many applications such as gas sensors, fuel cells and solar cells. The success of indium oxide in solar cell applications comes from its photon recombination

capability, allowing more electrons to pass through it surface, compensating for photons that are lost as heat or reflected due to low energy. In gas sensor applications, indium can combine with a range of molecules at the surface, allowing the detection of multiple molecules to occur.

As compared to ATO, it has higher electrical conductivity, resistivity, and reflectivity in the visible spectrum. Despite its success in visible spectra TCO applications, recent research has been performed to verify ATO as a replacement to indium tin oxide, or ITO. One of the main motives behind these efforts are the non-environmental friendly fabrication process and inefficient production cost related to ITO. In addition, elements, such as niobium (Nb) and copper (Cu), can be used as infrared reflective materials. This is dominantly because of the unique properties of pure SnO_2. While elements such as niobium (Nb) and indium (In) are used to dope SnO_2, calculations of the lattice parameter and grain size resulted in antimony (Sb) having a larger amount at low doping percentages. When in particle formation, the doping levels must be increased to create smaller crystallites, due to crystal growth suppression during calcination.[68, 69] However, through an intensive literature search, these results compared to the bulk material analyses have yet to be reported.

In recent research efforts, it has been shown that the combination of metal oxide sol gel with paramagnetic and ferromagnetic materials increases the uniform coverage and the infrared reflectivity.[38, 60, 70-72] In previous research, paramagnetic materials, such as tungsten and magnesium, and ferromagnetic materials, such as cobalt and iron, are added to metal oxide sol-gel solutions, such as chromium oxide and tin oxide. These materials are added in low concentrations to increase the magnetic properties as well as

enhance the infrared reflectivity. This is shown in sol-gel depositions by the investigation of the post-processing heat treatment.

It was presented by Xu et. al. [44] that Fe_3O_4 nanoparticles dispersed in a ferric hydrosol, or sol-gel solution, can be used to coat carbon fibers under vacuum pressure. In previous research, ferromagnetic oxide nanoparticles of 10-30 nm have been integrated into sol-gel solutions via magnetic stirring at temperatures below 40 °C. The immersion process was done several times with the annealing temperature at 120 °C. The optimal heat treatment temperatures were achieved at 300-550 °C. Previous research has shown the reflectivity of cobalt oxide sol-gels is not dominantly dependent on the heat treatment temperatures. However, the reflectivity of tin oxide sol-gel has been proven to be heat treatment temperature dependent in between 100-500 °C. Tin oxide has been used in multiple applications, such as solar cell junctions, optoelectronics, gas sensing, and electrochromic applications. It has proven to be a viable material for multiple applications because of its electrical conductivity, crystalline structure, visible light transparency, ultraviolet light absorption, as well as near and mid infrared reflection capabilities.[39, 73-75]

As previously stated, tin oxide has been doped with other materials, such as indium and fluorine, for many similar applications as antimony. However, for cost efficiency, better electronic structure pairing, and higher optical performances, antimony has been consistently chosen as the best material to dope tin oxide. While tin oxide has paramagnetic properties, antimony is diamagnetic. A material is defined as paramagnetic when the net magnetic moment is partially aligned in the direction of an applied magnetic field, and each atom acts as an individual magnet in a field. Comparatively, a material is

diamagnetic when the property of the orbital motion independently belongs to the individual electron in a field. This effect leads to negative susceptibility, or the lowering of the net moment in the material as an external field is applied.

Diamagnetism is only observed when the atom does not have a net spin or orbital moment. This causes weaker effects than paramagnetic materials. However, paramagnetic impurities often mask diamagnetic effects. This effect can commonly be seen in research such as electron paramagnetic resonance studies. It has been reported that higher doping levels of antimony increases the optical band gap, causing more interaction in the near and mid infrared region.[25, 27, 63, 76-79] Antimony causes this effect by increasing the amount of electrons in the conduction band and occupying vacant tin lattice sites. Concurrently, in ATO, while oxygen atoms migrate throughout the crystal lattice structure, antimony ions (particularly Sb^{3+}) migrate to the surface, increasing reflectivity and charge carrier concentration.

Mishra et. al. calculated the electronic band structure of antimony-doped tin oxide using the self-consistent-field scattered-wave molecular-orbital cluster approach.[80] From their results, it was concluded that conductivity could increase by way of thermal excitation. Therefore, their conclusions indirectly verified that the sol-gel annealing/heat treatment temperatures could be used as a conductivity tailoring mechanism. In previous research, magnetic oxide materials have been used for various applications, such as infrared reflective enhancement, microwave absorption, and mainly utilization of their intriguing magnetic-based properties. With all of the literature and research done on all of the ferromagnetic materials, a simple question arose, “Why chose cobalt oxide over iron oxide?” Table 3.4.1 lists some of the atomic characteristics of both materials. With

such a close comparison, the two materials perform slightly different, depending on the application. In this section, a discussion is given on why cobalt is a better candidate for this application. Next, ferromagnetics and their interaction in the near and mid infrared range are discussed. Also, cobalt's optical and thermal roles in the success of this research are discussed.

3.4. Ferromagnetic Oxides for Infrared Reflectivity Enhancement: Cobalt vs. Iron

Ferromagnetism in metals, i.e. the long range order of electron spins, must be reflected in the Fermi surfaces. They are split in a majority (spin up) and a minority (spin down) surface. The exchange interaction that lifts the spin degeneracy of the electronic bands translates in an analogous splitting in k-space. Above the Curie temperature a ferromagnet becomes paramagnetic and loses the ability to maintain a macroscopic magnetization. Therefore, the k-space volume that is enclosed by the two Fermi surfaces must be the same for spin up and spin down electrons. This is achieved if the exchange splitting of the bands that cross the Fermi level vanishes. It does, however, not mean that any magnetic moment disappears but that there is no more long range correlation between the magnetic moments on the lattice sites. Photoemission is able to observe the disappearance of the band splitting as well as local correlation effects above the Curie temperature, as they were observed with neutron scattering or core level photoemission.[81] The magnons, or spin waves, in the magnetic material cause a spatially periodic modulation of the permittivity of the medium, and the light is scattered by the permittivity fluctuations.

Table 3.4.1. Properties of iron and cobalt.

	Iron	**Cobalt**
Atomic Number	26	27
Mass	55.85	58.93
Electron Configuration	$3d^6 4s^2$	$3d^7 4s^2$
Melting Point (°C)	1530	1495
Boiling Point (°C)	2862	2927
Density, g cm^{-3}	7.87	8.90
Electrical Conductivity[e]	16	25

The electronic structure for iron and cobalt is shown in table 3.4.2. In terms of the electron structure, iron has a ($3d^6$, $4s^2$) electron structure, while cobalt has an electron structure of ($3d^7$, $4s^2$). The distribution of the electrons in the 3d and 4s shells are a function of their distance from the nucleus. Note that with the 3d electrons, the density of states is dense and close to the nucleus. The 4s electrons on the other hand, are spread out rather thinly and extend far from the nucleus where they can overlap orbitals of other atoms. For the case of iron, part of the electrons in the 4s band is transferred to the 3d band because of the overlap of the two bands. However, since the 3d+ band is already full, the excess electrons must go into the 3d- band reducing the net moment. The electronic distribution is important in this project because crystallography determines the degree of difficulty for for photons, or excited electrons to pass through the material.

Table 3.4.2. Electronic structure for iron and cobalt.

	Number of electrons in Following shells				
	3d+	3d-	4s+	4s-	Total
Iron	4.8	2.6	0.3	0.3	8
Cobalt	5	3.3	0.35	0.35	9

Cobalt oxide sol-gel thin films have been fabricated by various groups. From these experiments, it was shown that thicker layers provide higher crystallinity. As shown in chapter 4, this enhancing crystallinity effect is independent of annealing temperatures in the range of 100-500 °C. Concurrently, when used as a dopant at a constant thickness, cobalt oxide enhances the crystallinity of the sol-gel material prior to annealing/heat treatment. However, consequently, when thickness is a constant, there is a maximum limit to its crystallinity enhancing effects. It was reported by Drasovean et. al. that grain growth is observed by increasing the thickness and sol concentration [82]. Also, validation of direct and indirect transitions has been presented through X-ray diffraction, transmittance spectroscopy, and Swanepoel's calculation method of optical absorption and band gap energy differences. It has also been reported that the heat treatment atmosphere can be used to tailor the absorption coefficients. In the experiments conducted by Wang et. al., a nitrogen annealing environment was provided to cobalt thin films deposited by the spin coating method. Samples annealed at 300 – 600 °C were compared to samples annealed at 300 °C in nitrogen, both at atmospheric pressure.

By controlling the annealing environment, a reduction of oxygen and phase transition of Co^{3+} to Co^{2+} occurs. Also, the grain size calculated from the XRD data grows faster when compared to the results from in-air atmospheric temperatures. Calculated grain sizes from the Debye-Sherrer equation showed an increase from air to nitrogen environments with grain sizes measuring 21 and 26 nm for 400 °C and 500 °C. However, related reports also stated that this reduction of cobalt ions and rate of phase exchange were due to the presence of oxygen. Lower annealing pressures would allow for lower annealing temperatures and higher grain growth.

3.5. Thermal Effects of Heat Treatments on the Crystallography of Sol-gel Surfaces

Sol-gel depositions usually involve heat treatments or annealing cycles as a final processing step. Typically, the solvent is dried out of the sol-gel at a low temperature (~60-90 °C) before being raised to a heat treatment temperature suitable for that material (~200 – 1000 °C). Because of this process, studies have been conducted to reflect the electrical, chemical, and optical properties as well as the migration of atom during heat treatment. In doing so, analysis of the temperature affects on the surface is detrimental to the understanding of the heat treatment process. For ATO, the grain size of the thin film deposited material increases directly proportional to the heat treatment temperature. Atomic force microscopy reveals that the surface roughness increases when the sol-gel thin films are heat treated. This validates higher levels of crystallinity in heat treated sol-gel thin films. Also, reflections at specified angles from XRD measurements become higher in intensity when the films are heat treated at higher temperatures.[83, 84] Lattice

parameters can be calculated and evaluated for element identification, nearest neighbor calculations, and orientation identification. In addition to these effects, the measured resistivity of ATO thin films shows a correlating decrease. This affect has been attributed to the increase in charge carrier mobility and density.[83, 85]

3.6. Interaction of Sol-gels in Various Environment Conditions

Because of the nature of this application, the sol-gel coatings can be subjected to various elements of environment variations. Also, by temperature already being an important factor to the fabrication and performance of the sol-gel, it also determines the durability of the material. For instance, when in contact with water, hydroxylation may occur on the surface of the sol-gel, causing a bulk defect in the coating that can spread indefinitely across the entire coated surface. Hydroxylation occurs when hydroxyl groups of dissociated molecules form a layer on the surface of the material, followed by a layer of molecular absorption. Advantageously, tin oxide is very resistant to hydroxylation. Variations in high temperature and pretreatment with chemicals must be used to process tin oxide for such a desired reaction. Concurrently, Co_2O_3 reduces oxidation occurrences at different temperatures. The combination of these two materials increases the longevity of the sol-gel coating in high temperature or heavy moisture environments, making it extremely suitable for aerospace applications.

CHAPTER 4

UNDOPED AND COBALT-DOPED ANTIMONY TIN OXIDE SOL-GELS ON CARBON-SILICON LAYERS FOR MODELING SOL-GEL/CARBON FIBER INTERFACES

4.1. Introduction

This research presents a novel thermo-responsive sol-gel(dopant) combination and evaluation of the actuating responses due to various heat treatment temperatures. In this project, samples of antimony-doped tin oxide (ATO) doped with 0.1% cobalt oxide (0.1% Co_2O_3) sol-gel on carbon/silicon substrates are used to model the implementation of sol-gel coatings into carbon fiber composite systems. While ATO is a well-known transparent conductive material, the addition of cobalt oxide (Co_2O_3) alters its morphology and optical parameters at low annealing temperatures. By altering the ATO (0.1% Co_2O_3) heat treatment temperatures, the grain size starts to increase at 200 °C. However, when approaching 500 °C, Raman spectroscopy shows that the increase in intensity of ATO (0.1% Co_2O_3) is lower than ATO undoped. Scanning electron microscopy is used for imaging, and energy dispersive spectroscopy will be used for the composition analysis. Optical reflectance is reported via Fourier Transform Infrared

(FTIR) spectroscopy and Raman spectroscopy analysis. Recent military efforts in reflective composite design have become directed towards protection against infrared laser degradation to carbon fiber composites. In doing so, research efforts have been made toward modifying infrared reflective materials for implementation into carbon fiber composite systems.

In its pure form, tin oxide has become a material of interest because of its wide energy band gap of ~3.6 eV, high carrier mobility, absorption in the visible spectra, and its reflectance in the infrared spectra when doped with group III, V, and VII elements such as indium, antimony, and fluorine.[3] It has been proven that thin films of antimony-doped tin oxide (ATO) coatings show an increase in electrical and mechanical properties. It has also been shown that ATO has been proven to have high conductivity and high transparency in the visible range.[24, 25, 86, 87] Of most interest to this research, ATO also has beneficial reflective properties in the mid and far-range infrared spectra. In addition, ATO is oxidative resistant, and band gap tailoring capabilities are controlled by the doping level of antimony (Sb) and the heat treatment of the sol-gel solution. It has been theoretically proven that the antimony atoms in tin oxide lead to an impurity band with a significant free-electron-like characteristic, producing interesting optoelectronic properties.[80] Annealing temperatures have been shown to have an effect in altering optical properties in the electronic structure of ATO. Concurrently, the grain growth of cobalt (Co) in bulk and its parameters when interfaced with carbon after heat treatments have also been examined.[83] However, the implementation of Co as a dopant in antimony-doped tin oxide sol gel solutions to further enhance infrared reflectivity has not been reported.

In this work, sol-gel solutions of undoped ATO and ATO with a 0.1% Co_2O_3 dopant level [ATO (0.1% Co_2O_3)] are deposited on carbon/silicon substrates and were measured for their chemical composition consistency by energy dispersive X-ray spectroscopy (EDS). The samples were examined by Fourier transform infrared (FTIR) and Raman spectroscopy for phase shifting in the crystal structure. The analyses verify the composition of the samples and provide insight on how Sb and Co atoms perform after undergoing a variation of heat treatment temperatures. The enhancing effect of cobalt oxide (Co_2O_3) as a dopant in ATO sol-gel coatings on carbon surfaces at low annealing temperatures (200-300 °C) is presumed to be caused by the crystallinity of the materials, the increase in grain size, and the low degradation of phase composition.

4.2. COMSOL Finite Element Analysis Simulation of Sb-doped SnO_2 Thin Films

The simulation results shown in figure 4.2.1 show the temperature change and radiosity, surface irradiation, and reflectivity. Radiosity is an optics and heat transfer parameter in finite element analysis that represents the total radiation intensity leaving a surface. This parameter considers the radiation being emitted by the surface and reflected from the surface. Combining these two factors into one term allows the simulation software to determine the net energy exchange between multiple surfaces. Table 4.2.1 shows the simulation parameters. The model simulates the lamp as a solid object with a volume heat source of 25 kW.

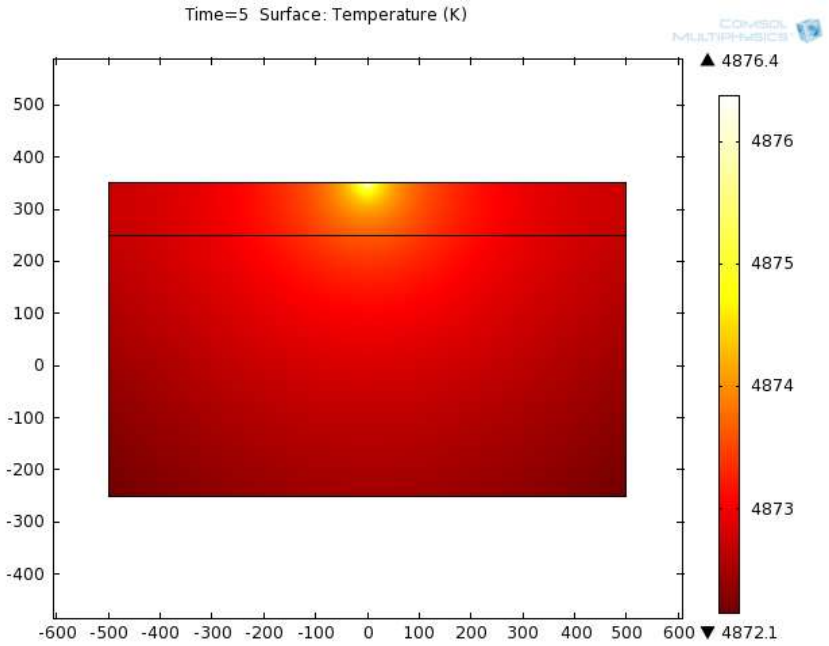

Figure 4.2.1. Two dimensional color graph showing the temperature change in the interfaces at maximum exposure from the Nd:Yag laser point source.

Table 4.2.1. COMSOL finite element simulation parameters.

Parameter	**Value**	**Description**
T_wall	400[K]	
T_gas	400[K]	
h_gas	20[W/(m^2*K)]	Heat transfer coefficient
k_sens	27[W/(m*K)]	Thermal conductivity sensor
rho_sens	2000[kg/m^3]	sensor density
Cp_sens	500[J/(kg*K)]	sensor heat capacity
e_sens	0.8	sensor surface emissivity
k_lamp	400[W/(m*K)]	lamp thermal conductivity
rho_lamp	8700[kg/m^3]	Lamp density
Cp_lamp	10[J/(kg*K)]	lamp heat capacity
e_lamp	0.99	lamp surface emissivity
q_lamp	60[kW]/(pi*50^2*1[mm^3])	lamp heating power
e_oxide	0.05	wafer surface emissivity
ampl	50	IR amplification factor sensor

It is insulated on all surfaces except for the top, which faces the oxide layer. At this surface, heat leaves the lamp as radiation only. In order to capture the heat source's transient startup time, the model uses a low heat capacity, C_p, for the solid (10 J/(kg·K)). In our simulations, it is assumed that the oxide layer dissipates energy via radiation and convection on all surfaces. The temperature probe is placed on the carbon/SnO_2 interface, and the simulation results graphed both temperature and radiation. The thermal material properties are set to parameters set in the COMSOL material database. The point source intensity was raised at 0.1 mW per second. As seen in the plotted results in figure 4.2.2, the thickness of the tin oxide determined the level of reflectivity. Within 0.05 µs, the different thicknesses reflected various amounts of infrared light.

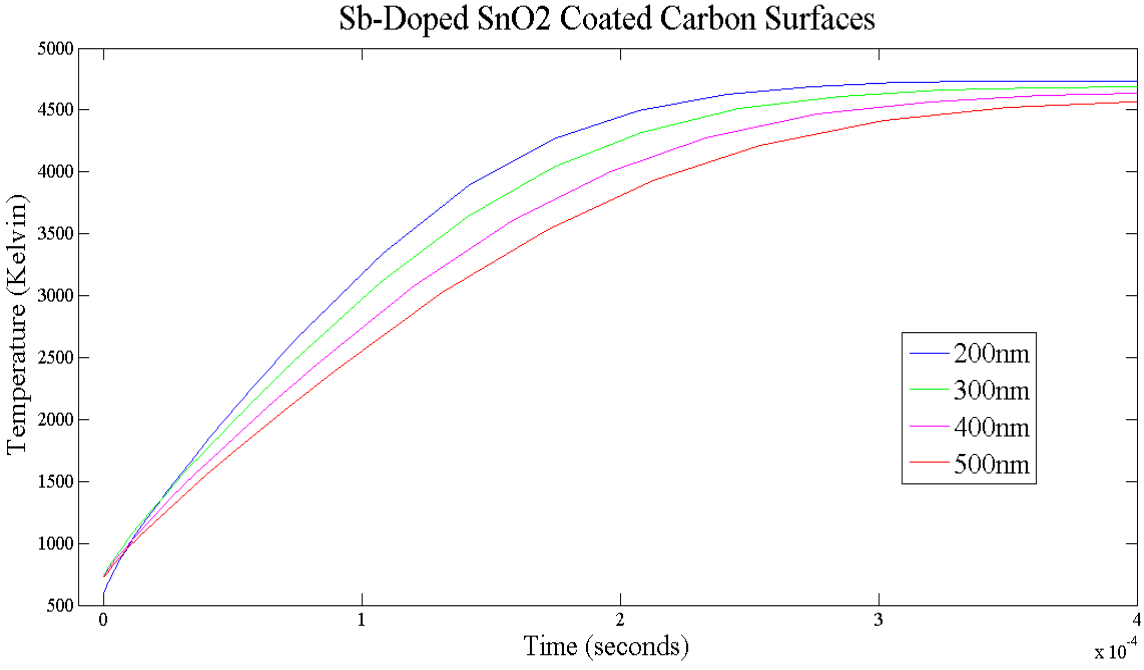

4.2.2. Reflectivity of tin oxide coated carbon surfaces versus time.

4.3. Experimental Procedure

The ATO and ATO(0.1%Co_2O_3) sol-gel solution was made with a mixture of oxide sol-gel solutions. All of the sol-gels were made with 2-ethylhexanoic acid. The ratio of cobalt and antimony to tin are as follows:

- Co_2O_3:SnO_2 = 0.0011:1
- Sb_2O_3:SnO_2 = 10:90

Silicon wafers of 300 mm diameter were cleaned using a standard wafer cleaning process, which removed organics, native oxide layers, and ionic contamination. The wafers were then cut into 1 x 1 cm^2 squares. A lead target was used to sputter 10-20 nm of carbon onto the silicon substrate at 50 mTorr. In each deposition, roughly 25 nm of carbon were deposited on a silicon substrate. 20 μL of the sol-gel solution was deposited on the sample surface by spin coating at a rate of 2000 rpm for 20 s.

A programmable Vulcan 3-550 box furnace (120 V/ 12 A) was used to perform the heat treatments. The samples were heat treated in the temperature range of 200-500 °C at atmospheric pressure. In each heat treatment, the samples were ramped up to the specified temperature at a rate of 10 °C/min. Three time and temperature intervals were chosen to assure the evaporation of the sol and highest possible sol-gel layer quality. Once reached, the specified temperature was held for 1 h. The samples were allowed to cool to room temperature for a minimum of 4 h before testing. Figure 4.3.1 shows a two-dimensional layout of the sample.

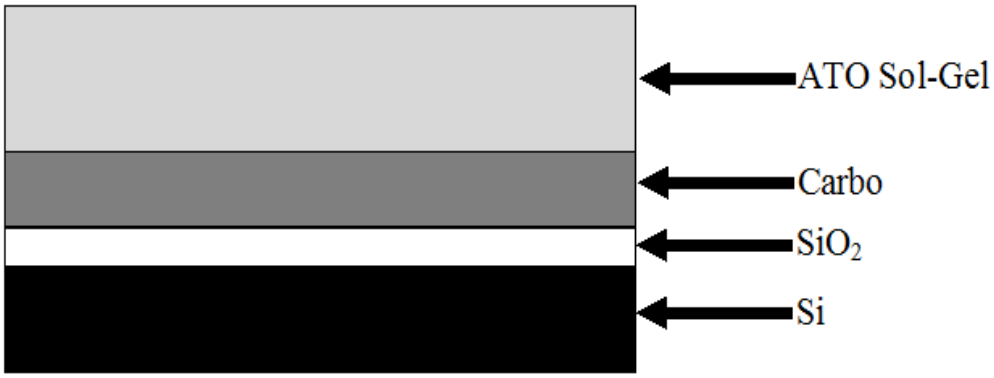

Figure 4.3.1. A diagram of the ATO sol-gel/carbon/silicon sample layouts used for electrical testing is shown.[88]

4.4. Imaging Analysis

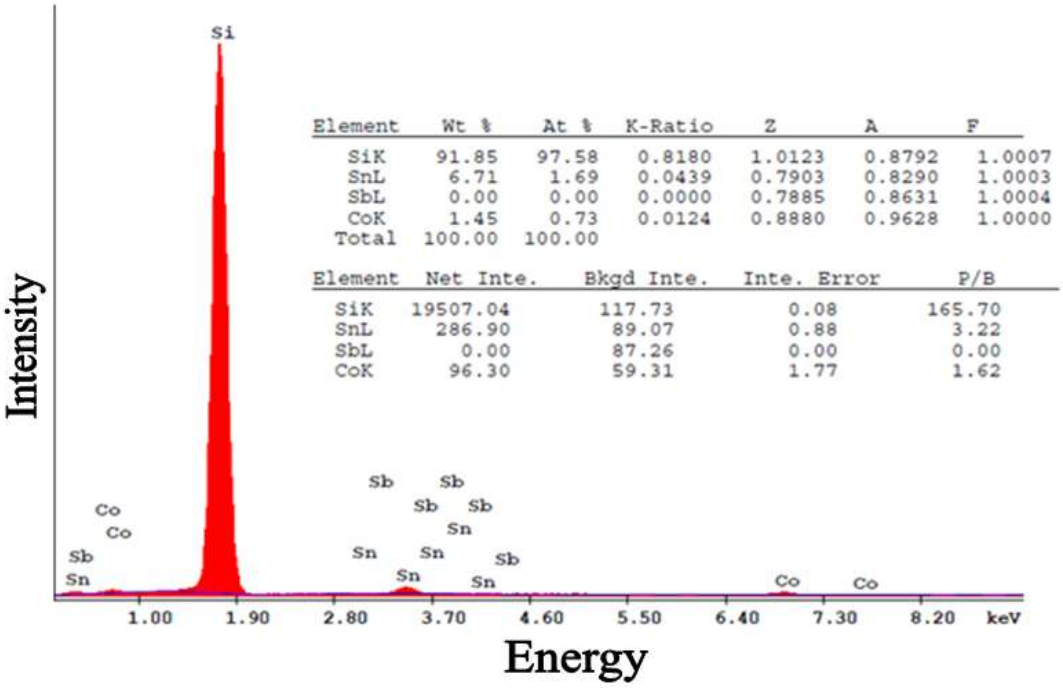

Figure 4.4.1. EDS quantitative element composition analysis of ATO(Co_2O_3) after 500 °C heat treatment.[88]

Imaging and EDS were done on a Hitachi S-800 scanning electron microscope with an EDAX-Phoenix EDS detector. Fig. 4.4.1 shows the EDS results. It is noticed that there are no visible single oxygen peaks. This is because the oxygen (O) is at a lower intensity than tin (Sn) and Co, which causes the O peaks to be hidden behind the Sn and Co peaks. In the ATO sol gel solution, the oxygen content was only added 1-5% relative to Sn, and Sb was 0.5 %. To this solution, Co_2O_3 was added at 0.1 %. However, because of its energy, the K- and L-shell peaks of Sb and Sn were independently identified.

4.5. Optical Analysis

4.5.1. FT-IR Analysis

FTIR spectroscopy was performed to evaluate the effects of heat treatment to the sol-gel reflectivity. From the results shown in figure 4.5.1, it is seen that the heat treatments can be used as a tuning procedure for a specific amount of reflectance. The increase in reflectance by way of the annealing temperature is attributed to the increase in grain size. Specifically, this affect is mainly due to an increase in the thermal energy for crystallization, recrystallization, and growth of grains in the films. Structural parameters, such as dislocation density and the micro-strain are found to show a decreasing trend with increase in annealing temperature, which may be a result of the reduction in the concentration of lattice imperfections.[32] In addition, ATO is oxidative resistant, and band gap tailoring capabilities are controlled by the doping level of Sb and the heat treatment of the sol-gel solution.

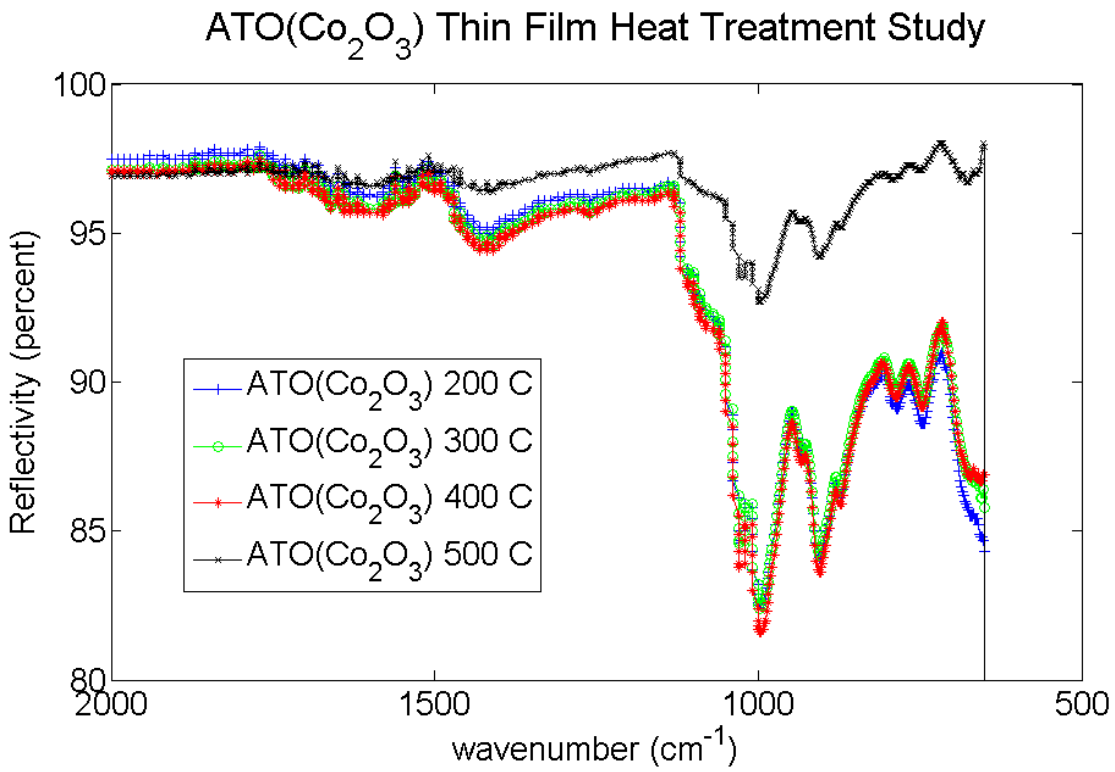

Figure 4.5.1. -IR spectra of ATO(Co_2O_3) heat treated from 200 – 500 °C.

4.5.2. Thin Film Analysis – Raman Spectroscopy

Figure 4.5.2 shows the analysis of the ATO sol-gel thin films heat treated at 200 and 500 °C. From the experiments, it is seen in figure 4.5.2 that the (Sb)SnO_2 coating does, in fact, experience higher lattice vibrations in the crystal lattice due to the performed heat treatment. It is shown that the vibrations in the crystal lattice increase after the heat treatment at 500 °C. This is attributed to the increase in grain size growth and shifting of the antimony atoms towards the surface. During the heat treatment, Sb forms ionic bonds with the SnO_2 lattice, substitutionally replacing Sn defects and dislocations. It has been shown in previous research [89] that, during the heat treatment, antimony atoms approach the surface, while oxygen increases the charge carrier mobility

for tin. When photons collide with the lattice points, fewer electrons at a lower energy level are observed.[88]

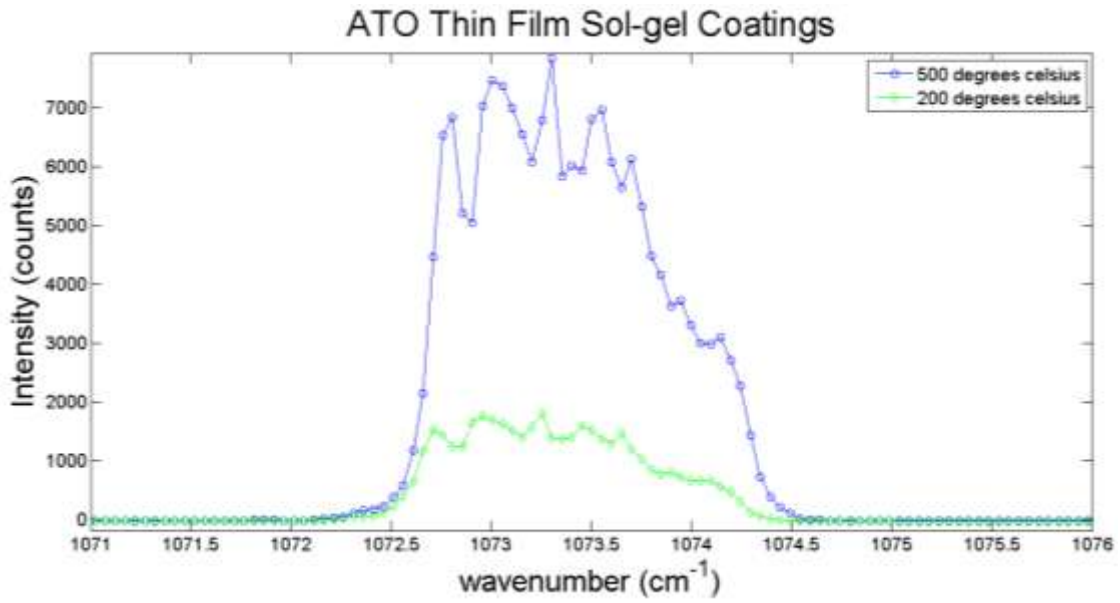

Figure 4.5.2. Raman spectroscopy of ATO sol-gel thin films heat treated at 200 and 500 °C.

The change in intensity indicates the polarization change of atoms at the surface. Therefore, it is presumed that the migration of Sb towards the surface and the increased charge carrier mobility of Sn causes the change in grain size boundaries in the ATO thin films annealed at 500 °C as compared to 200 °C. Collectively, he increase in reflectivity is correlated to the grain size growth and increase in atom density at lattice sites.[83] As seen in figure 4.5.3, it is seen upon visual inspection that the coating surface has a dark blue appearance after the heat treatment. Distinction in between heat treatment and color shade were negligible. Previous reports also agree with the assumption that this is also due to the redistribution of atoms and configuration of the electronic structure.

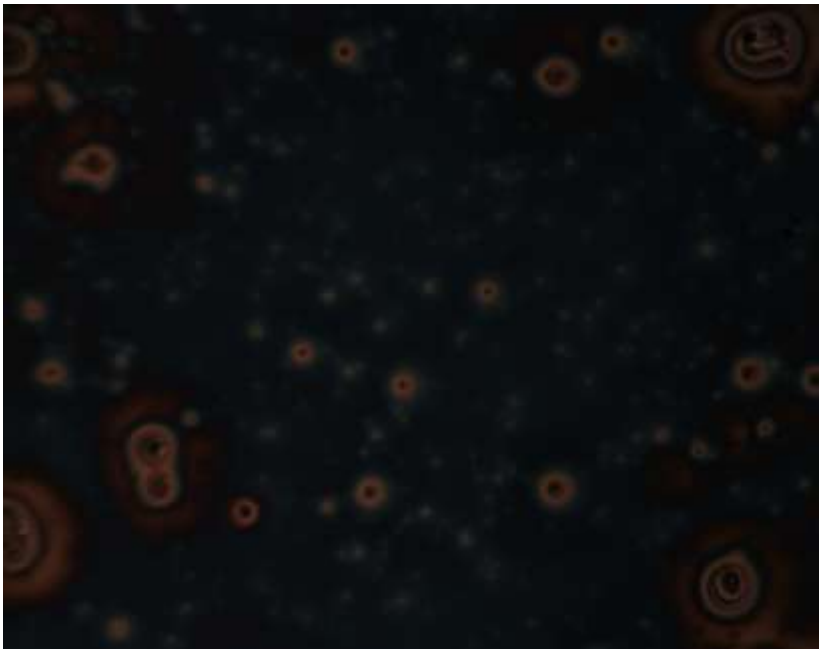

Figure 4.5.3. ATO(0.1%Co_2O_3) after a 300 °C heat treatment.

Raman spectroscopy graphs in figures 4.5.4 and 4.5.5 show undoped ATO, Co_2O_3, and ATO (0.1% Co_2O_3) after 200 and 500 °C, respectively. Both ATO (0.1% Co_2O_3) samples after 200 and 500 °C heat treatments showed high vibrations in the lattice in the 1072-1075 cm^{-1} range. The Co_2O_3 sol-gel thin film remains consistent throughout the heat treatment range. After heat treatment on the ATO (0.1% Co_2O_3) samples, the Sb and Co atoms form ionic bonds. The intensity change of ATO and ATO (0.1% Co_2O_3) at higher heat treatment temperatures indicates the polarization change of atoms present at the surface. When photons collide with the lattice points, fewer electrons at a lower energy level are observed.

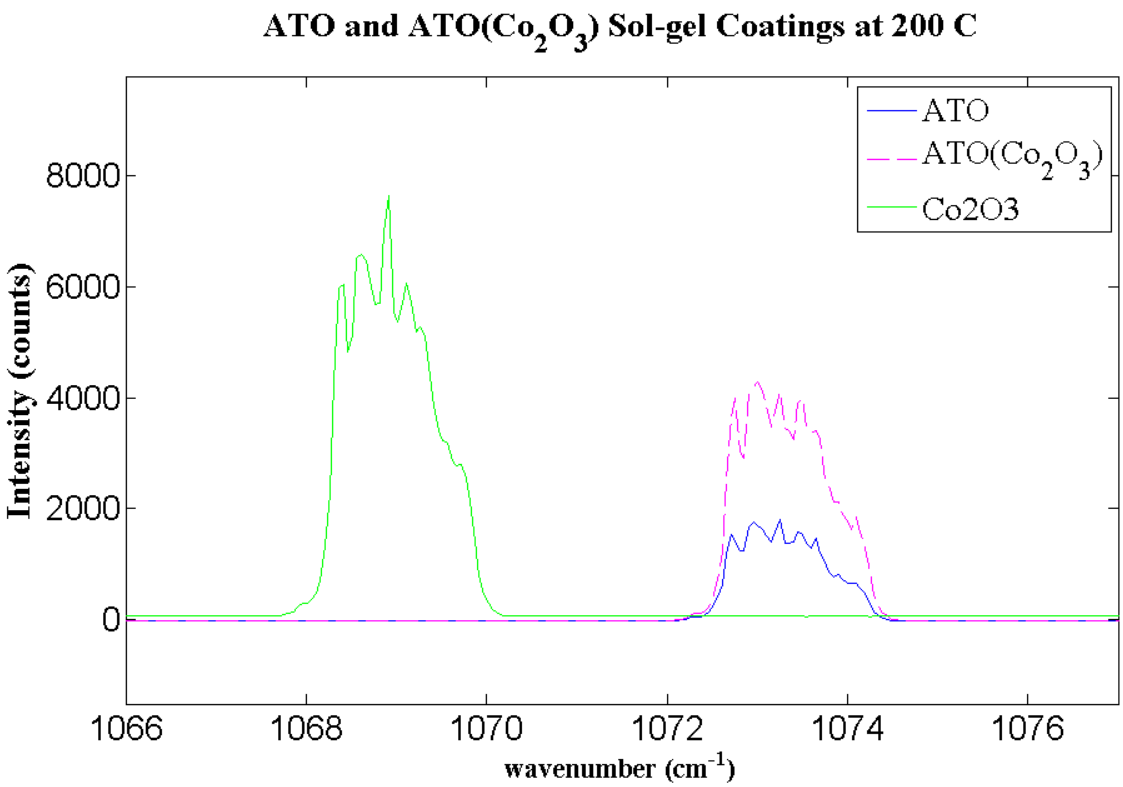

Figure 4.5.4. Raman spectroscopy of ATO(Co_2O_3) after one cycle of spin coating/heat treatment at 200 °C.[88]

The cobalt oxide films show similar Raman spectroscopy responses to that of Pal, et. al.[90] The increase in wavelengths is directly proportional to the increase of reflectivity of Co_2O_3. During the recombination and process, Sb and Co are diffused through the crystal structure by way of Sn dislocations and O deficiencies, Sb^{3+} ions segregate towards the surface.[36] Previous studies have implied that Co^{2+} substitute the Sn^{2+} ions and O octahedral coordinated cation sites.[89] Therefore, it is presumed that the Co atoms at the surface cause the slower rate of grain size increase in the ATO (0.1% Co_2O_3) thin films at 500 °C as compared to 200 °C.

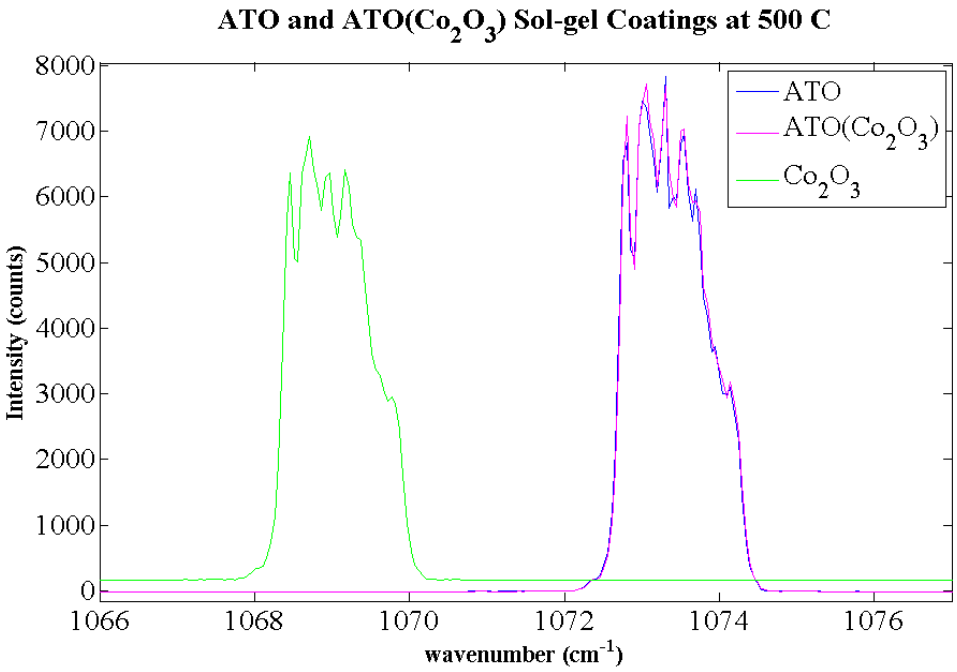

Figure 4.5.5. Raman spectroscopy of ATO(Co_2O_3) after one cycle of spin coating/heat treatment at 500 °C.[88]

4.6. Discussion

As seen from previous reports, ATO forms a tetragonal crystal lattice structure upon deposition [91, 92]. During the heat treatment, the crystal structure is deformed, and Sn^{3+} ions create dislocations and defects in the crystal structure. Concurrently, the grain sizes of Sn and Sb increase, causing a higher percentage of reflectivity. The addition of Co_2O_3 appears to slow the grain size growth at ~500 °C, as opposed to the undoped ATO thin film that has comparable reflectivity at this temperature. This reaction is attributed to the Sb^{3+}, Sb^{5+}, and Co^{2+} ions replacing Sn^{3+} ions in the lattice structure.[92] The substitution of Sn ions for Sb and Co ions is possible because of the similar ionic radii (Sn = 0.071 nm, Sb = 0.065 nm, and Co = 0.071 nm). For the effect of the added dopant, it has been reported that Co can have altered properties based upon the

roughness of the carbon surface. In previous research, the interfacial reaction between cobalt and carbon based on the deposition temperature has been examined. It was shown the crystallinity of cobalt was affected from deposition from temperatures as low as room temperature and 250 °C. Therefore, it can be concluded that, even at low dopant levels, cobalt will show a variation of crystallinity and can be correlated to the optical parameters based upon the given heat treatment temperature. This further proves that the consistency and roughness of the coating is controlled by the heat treatment temperatures. Furthermore, the collective data from Raman spectroscopy and FTIR shows that the optimal heat treatment temperatures for maximum reflectivity from ATO (0.1% Co_2O_3) sol-gel thin film coatings is between 200-400 °C.

4.7. Conclusion

Optical properties of ATO (0.1% Co_2O_3) can be altered by various heat treatment temperatures. Results show that Sb^{3+}, Sb^{5+}, Co^{3+}, and Co^{5+} ions substitute Sn^{3+} ions in the crystal structure, promoting changes in polarization and altering reflectivity. Higher heat treatment temperatures allow more Co^{3+} and Sb^{3+} ions to merge into the crystal, replacing more Sn^{3+} dislocations and defects. Future work includes investigation of Co_2O_3 at higher doping levels and higher heat treatment temperatures. Future work will also include examining the magnetic properties of cobalt as a dopant inside the sol-gel composites.

CHAPTER 5

INFRARED REFLECTIVE COATINGS OF ATO SOL-GELS ON CARBON FIBERS

5.1. Introduction

Previous research has shown the capability to reflect or absorb specified wavelengths of light by functionalizing various materials [2, 47]. From these research advancements, materials have been used in multidisciplinary applications such as telecommunications [20], environmental protection[21], and renewable alternative energy[3]. While the application of incorporating reflective sol-gels being incorporated into composites has been examined in previous research [47], literature is limited to selective types of dopants being added to metal oxide sol-gel solutions [48, 76, 93-97]. In its pure form, tin oxide (SnO_2) has become of interest to researchers because of its wide energy band gap of ~3.6 eV, its high carrier mobility, its absorption in the visible spectra, and its reflectance in the infrared spectra when doped with group III, V, and VII elements such as indium, antimony, and fluorine [3, 38, 68]. Antimony-doped tin oxide (ATO) is a well-known transparent conductive material and has been used in many thermal, optoelectronic, and solar applications. For specified optical applications such as laser lens coatings, fiber optics, and electrochromic devices, ATO can serve as an

actuator capable of reflecting infrared radiation in the infrared wavelengths of 0.7 – 1.2, 3 – 5, and 8 – 12 μm. Composites containing antimony-doped tin oxide (ATO) coatings show an increase in electrical and mechanical properties. In multiple deposition techniques and analysis, high conductivity, low resistivity, and high transparency were obtained ATO films in the visible range [27, 89, 98]. ATO also has beneficial reflective properties in the near and mid-range infrared spectrum (620-640 nm). These properties allow ATO to be implemented into designs and systems for electrochromic displays, laser lenses, solar panels, and electronic devices. Annealing temperatures have been shown to have an effect in altering electrical and optical properties in the electronic structure and the grain size of ATO when interfaced with carbon thin films [4, 83]. This research presents the investigation of ATO sol-gel coatings on carbon fibers for its implementation in infrared reflective carbon fiber reinforced composites. The main investigation lies within the infrared laser interaction with the surfaces of the sol-gel thin films and coatings. An analysis of the heat treatment temperature effects is given, followed by a composition and optical analysis and discussion.

5.2. Experimental Procedure

The ATO and sol-gel solution was made with a mixture of oxide sol-gel solutions. All of the sol-gels were made with 2-ethylhexanoic acid. The ratio of antimony oxide to tin oxide is Sb_2O_3 : SnO_2 = 10: 90. Benzene, and active solvent, was used to assist in the adhesion process, as graphene is commonly described as benzene stripped from its

hydrogen bonds[83]. The procedure used for the sol-gel thin film deposition is referenced here [88].

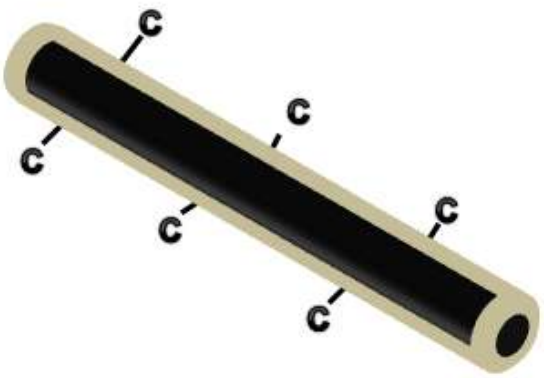

Figure 5.2.1. A three dimensional drawing of the carboxyl bonds after a nitric acid wash.

The procedure for coating the carbon fibers is as follows:

1. Carbon fibers were immersed in an ethanol:acetone (1:1 ratio) solution for 2 hours.
2. The fibers were dried in ambient air at atmospheric pressure for a minimum of 1 hour.
3. Next, the fibers were placed in nitric acid (HNO_3) for 2 hours. By doing so, carboxyl, carbon monoxide, and hydroxide bonds were created on the carbon fiber surface. Therefore, this step promotes adhesion between the sol gel solution and the carbon fiber surface. A three dimensional drawing is shown in figure 5.2.1.
4. Next, the fibers were allowed to dry 2 hours in ambient air.
5. The fibers were immersed in the (Sb)SnO_2 sol-gel solution for 4 hours.

6. Lastly, the fibers were dried in the temperature range of 200-450 °C for 4 hours in air.

Figure 5.2.2 shows the coated carbon fibers after the sol-gel coating process.

Figure 5.2.2. Piece of interweaved 0°/90° carbon fiber mat.

5.3. Surface Analysis – Scanning Electron Microscopy and Electron Diffraction Spectroscopy

Imaging and electron diffraction spectroscopy (EDS) were done on a Hitachi S-800 scanning electron microscope with an EDAX-EDS detector. Scanning electron microscopy results are shown in figures 5.3.1 through 5.3.3. It is noticed that there is a consistent coverage of sol-gel coating throughout the carbon fiber mat. Also, from these images, the diameter of the individual carbon fibers were measured, which ranged from 4 – 7 μm.

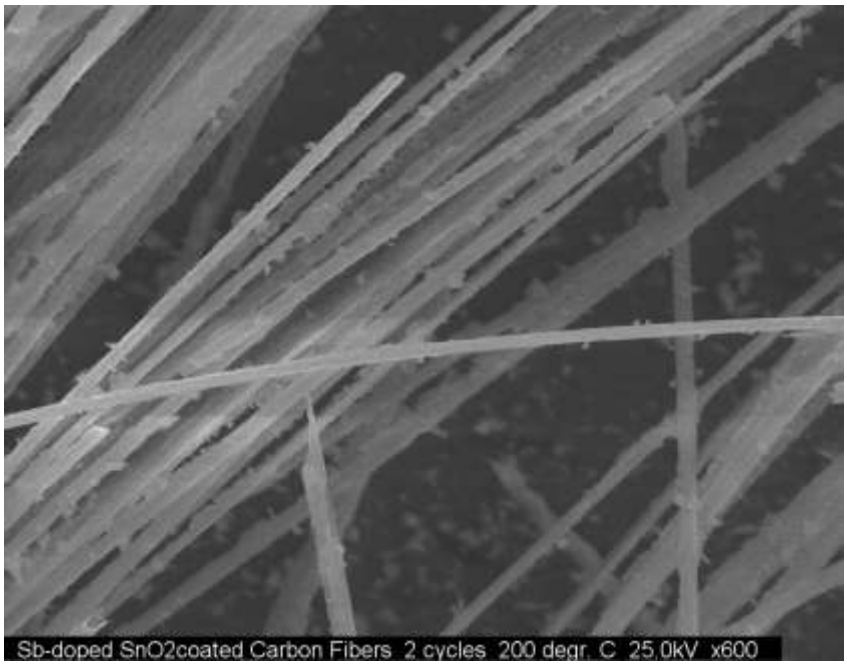

Figure 5.3.1. ATO coated carbon fibers heat treated at 200 °C.

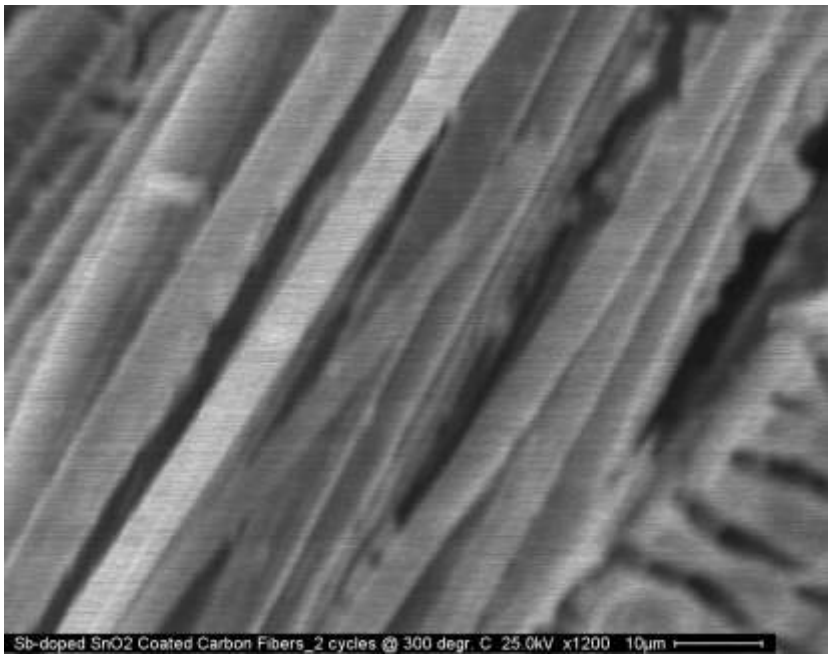

Figure 5.3.2. ATO coated carbon fibers heat treated at 300 °C.

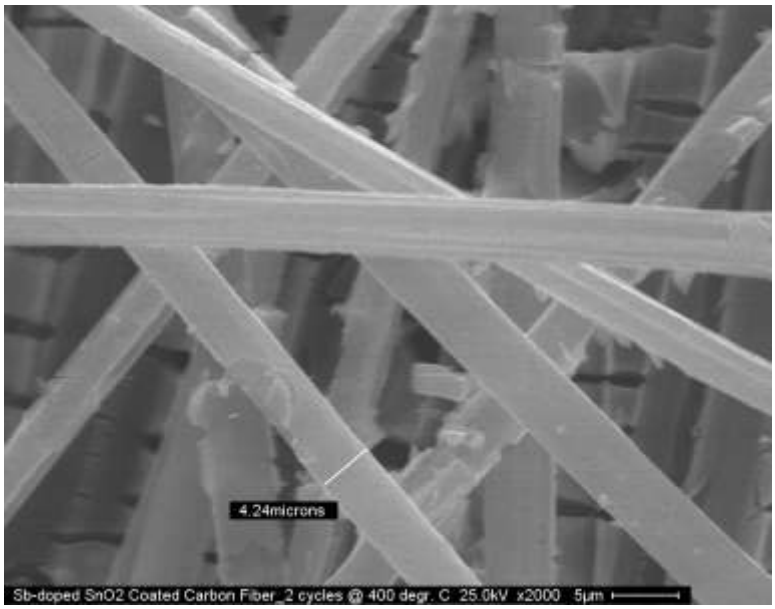

Figure 5.3.3. ATO coated carbon fibers heat treated at 400 °C.

The coated carbon fiber diameters ranged from 6 – 10 µm. While sol-gel coating coverage is highly consistent, a distinction of coverage could not be identified through the heat treatment temperature study. It was also identified that, because of the multiple coatings on a bulk scale, defects and micro-strains in the sol-gel surface were visible. This was attributed to the heat treatment process. Small defects and cracks in the surface can be covered and corrected by multiple coating cycles. In the SEM/EDS pictures in figure 5.3.4, it is seen that the entire fiber is coated with a high degree of uniformity with some areas of sol-gel agglomeration. The consistency and roughness of the coating is attributed by the heat treatment temperatures. However, the consistency and roughness of the coating is controlled by the heat treatment temperatures.

The main SEM image can be reconstructed by lining up all of the photos of the individual elements shown from EDS. Consistent vacancies, or dark spots, on every EDS

element image show where the other elements dominate on the surface. For the samples imaged, two cycles of immersion/drying/heat treatment were completed. The immersion time was 1 hour, the room temperature drying was 4 hours. The heat treatment time was maintained at 2 hours.

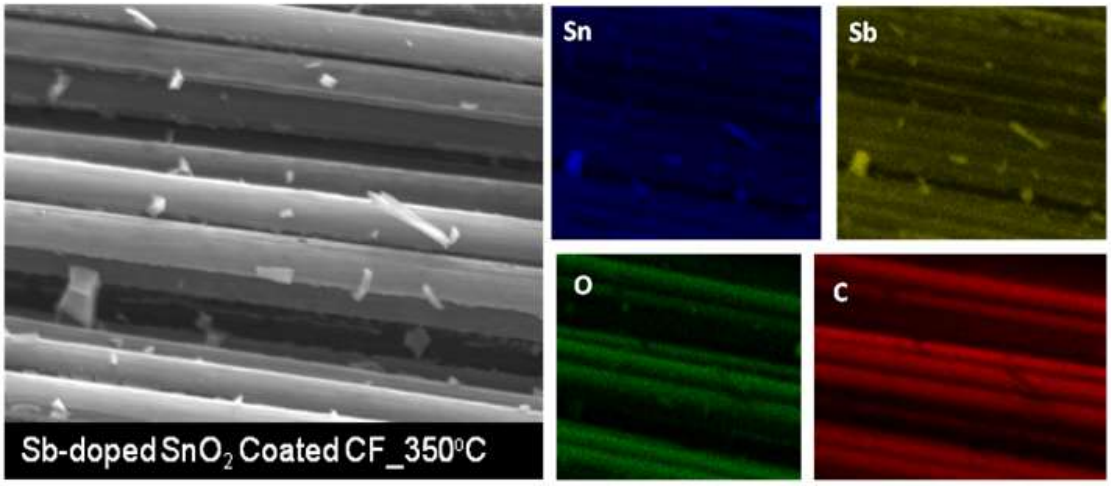

Figure 5.3.4. SEM and EDS color mapping of (Sb) SnO_2 coated carbon fiber mat (2a). Sn(2b), antimony(2c), oxygen(2d), and carbon (2e) have been identified in the sample separately.

Figure 5.3.5 shows the EDS quantitative analysis of the Sb-doped SnO_2 coated carbon fibers. It is noticed that there is only one visible single oxygen peak. This is because the k-shell peaks are hidden behind the Sn and Sb peaks. Also, a majority of the Sb peaks are blended with the Sn peaks due to their very close l and k-shell energies. In the crystal lattice of SnO_2, oxygen is interstitial, and the dopant, Sb, takes advantage of its placement to combine with the crystal lattice. In the Sb-doped SnO_2 sol gel solution, the oxygen content was only added 1-5% relative to Sn, and Sb was 0.1-0.5 %.

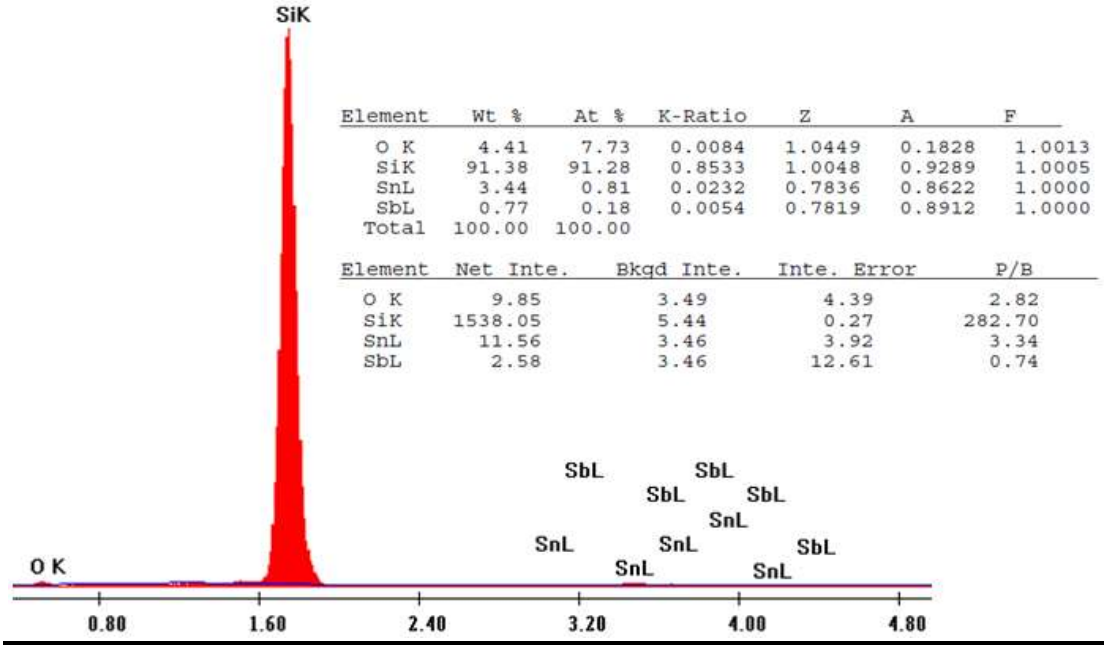

Figure 5.3.5. EDS mapping of ATO thin film sample heat treated at 200 °C.

5.4. Optical Analysis of ATO Sol-gel Coated Carbon Fibers – FT-IR Spectroscopy

FT-IR spectroscopy was performed on a Nicolet 6700. Analysis in figure 5.4.1 shows that the fibers increase in reflectivity when using higher temperatures during the heat treatment. FT-IR was chosen as an alternative method of optical characterization because of its functionality of scanning the entire sample surface and providing an integrated reading of reflectivity. Raman spectroscopy analysis of the coated carbon fibers resulted in inconsistent readings, as the conformal surface and heat-induced coating defects caused fluctuations in measurement. Prior to deposition, a nitric acid and acetone wash was given to the carbon fiber mats. By doing so, carboxyl, carbon monoxide, and hydroxide bonds were created on the carbon fiber surface.

Therefore, this step promotes adhesion between the sol gel solution and the carbon fiber surface. By atomic bonding nature, ATO forms a tetragonal crystal lattice. [92]. While oxygen is identified as the dominate donor of electrons in the system, Sb^{3+} and Sb^{5+} ions substitute Sn^{4+} ions in the lattice structure [36], further promoting electron mobility and bonding between the Sb and Sn atoms. Also, previous work has proven that Sn^{4+} ions create dislocations and defects in the crystal structure due to their migration through the crystal structure. Because of this behavior, Sb^{3+}, Sb^{5+} ions replace Sn^{4+} ions in the lattice structure substitutionally.

The substitution of Sn ions for Sb ions is possible because of their similar ionic radii (Sn = 0.071 and Sb = 0.065). The FT-IR studies performed by J. Zhang, et. al.[99] agree with the presented results, showing that the Sb ions substitute easily into the SnO_2 structure due to the Sn–O bond length, which occurs at ~600 cm^{-1}. Sb's duplicate oxidation states, Sb^{3+} and Sb^{5+}, causes a shift in the Sn–O vibration feature.[99] Concurrently, previous results have also shown that the Sb atoms migrate to the surface, dominating the optoelectronic response[36]. From these results, it is hypothesized that, even at low dopant levels, Sb will show a variation of crystallinity and can be correlated to the optical and electrical behavior. However, the consistency and roughness of the coating is controlled by the heat treatment temperatures. The observed enhancing effect from heat treatment/annealing temperature variation is presumed to be caused by the crystallinity of the materials, the available amount of carboxyl bonds, and the low degradation of phase composition in high temperatures. Results agree with previous reports that higher heat treatment temperatures allow more Sb^{3+} and Sb^{5+} ions to merge into the crystal, replacing Sn^{4+} dislocations and defects.

5.5. Conclusion

In conclusion, this work shows results of sol-gel solutions of ATO deposited on carbon fibers and measured for their morphology and optical properties. Based on the heat treatments at specified temperatures, a trend of increasing reflectivity and alteration in the crystal structure was observed. FT-IR spectroscopy was used to characterize the material composition and infrared reflectance in the infrared spectra. The tin peaks were observed, and the reflectivity increase was correlated to the heat treatment temperature. Scanning electron microscopy and electron diffraction spectroscopy were used for surface imaging and element analysis, respectively. The qualitative EDS analysis identified the amounts of tin, antimony, and oxygen present. SEM images showed a secondary image of the coated carbon surface, and were used to center the image for EDS color mapping. The color mapping of each element verified the presence and location of each element at a submicron magnification. FT-IR spectroscopy was used to characterize the material composition and infrared reflectance in the infrared spectra. Scanning electron microscopy and electron diffraction spectroscopy were used for surface imaging and element analysis, respectively.

CHAPTER 6

OPTICAL EFFECTS OF Co_2O_3 DOPING LEVELS IN ATO SOL-GELS ON CARBON FIBERS

6.1. Introduction

This research presents a novel thermo-responsive sol-gel(dopant) combination and the evaluation of infrared reflectivity due to changes in doping levels and incident angles of reflection In this project, samples of antimony-doped tin oxide doped with cobalt oxide (ATO($x\%Co_2O_3$) $0.2<x<0.5$) sol-gels were used to coat three inch interwoven carbon fiber mats. These coated mats were heat treated at 250 °C and then tested for their reflectance via angle-dependent measurements. The targeted spectra of interest was 0.7 – 2.3 μm. Scanning electron microscopy is used for imaging, and energy dispersive X-ray spectroscopy will be used for the composition analysis. Hemispherical total reflection was conducted, and the ATO ($5\%Co_2O_3$) coating gave, while the angular dependent reflectivity measurements are conducted using a modified FTIR setup.

Recent military initiatives, such as the Airborne Laser (ABL) and Advanced Tactical Laser (ATL) programs have expressed interest in the design of infrared laser-based defensive systems. These systems share the objective of locating a munitions

target, tracking the trajectory, and then destroying the target prior to reaching its desired destination. These objectives are accomplished by the use of a network of lasers operating in the infrared spectrum at a 1.31 μm wavelength. In the process of destroying the target, the laser shines on the surface, conforming to its surface and causing inadvertent combustion. The development of these lasers has led to interest in materials that are able to reflect infrared energy, specifically, sol gel coated carbon fibers. Also, the effectiveness of the lasers become of concern on conformal surfaces, which may degrade the lasers' surface damage capabilities. Investigations of these materials can provide an experimental view on how the reflective coatings will perform when used as a thermal infrared reflective shielding.

In new studies, novel materials are being designed and implemented into composite designs to increase reflectivity and dissipate thermal heat at specified wavelengths. In previous work, reflection and absorption of specified wavelengths has been demonstrated by various materials on the micro and nanometer scale.[65, 100] The thermal infrared radiation reflective property of the selected materials is mainly based on low emissivity. In common practice, low-emissive coatings can reflect 85-95% of the thermal radiation while still allowing 60-65% transmittance of specified optical wavelengths.

As shown through this research, while many methods can be used to deposit ATO, the sol-gel method is preferred, because of its capability to create molecularly homogeneous solutions, its low temperature processing requirements, and the versatility of adding uncommon dopants that can be included in solution. In related research, the sintering, or heat treatment, and temperature of the substrate have been investigated for

their influence on the deposition of ATO.[101] Work performed by Zhu and Jiang has shown that the combination of metal oxide sol gel with ferromagnetic materials.[102] It was shown that the crystallinity and resistivity is directly affected by its calcination, or heat treatment, temperatures. While the addition of ferromagnetic materials into ATO has been examined in previous research, the literature is limited to a selective amount of dopants. Figure 6.1.1 gives an illustration of the infrared reflective carbon fiber mat design.

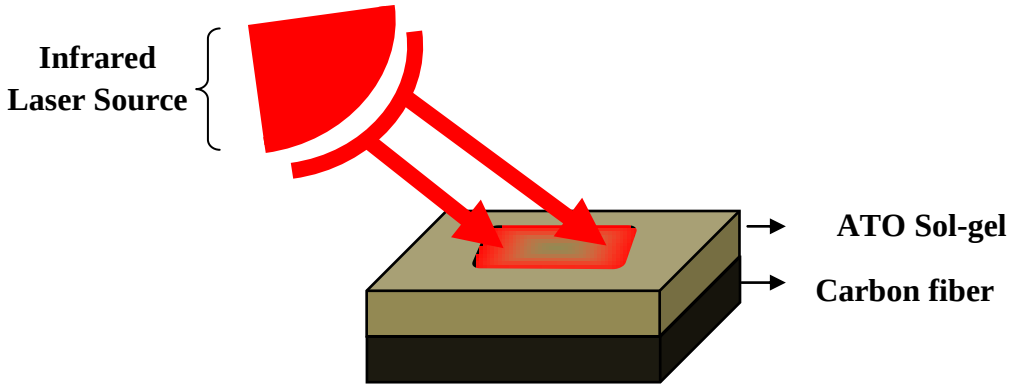

Figure 6.1.1. An infrared laser from a monochromatic infrared light source penetrating the surface of ATO/carbon fiber.

In this set of experiments, the hemispherical reflectance and angular dependency of reflectance of cobalt oxide-doped ATO (ATO(x%Co_2O_3), where 0.2<x<0.5) sol-gel coatings on carbon fiber mats were investigated. Alteration in reflectance is correlated to the doping levels of Co_2O_3. The hemispherical reflectance is conducted to give an integrated 180° reflectance at a specified incident angle of 10°. Concurrently, angular dependent angles examine the sol-gel coatings from its incident specular angle of ~ of 45° and alter this angle ±5° and ±10°. It is observed that the reflectance sol-gel varies

based on the incident angle of the laser source. We present a detailed discussion of our results, describing how it correlates with previous reports and how new conclusions are made.

6.2. Experimental Procedure

The ATO(x%Co_2O_3) sol-gel solutions were made with a mixture of oxide sol-gel solutions. All of the sol-gels were made with 2-ethylhexanoic acid. The ratio of cobalt and antimony to tin are as follows:

- Co_2O_3:SnO_2 = 0.0011:1
- Sb_2O_3:SnO_2 = 10:90.

In our customized method of sol-gel solution fabrication, tin alkoxides were used as the salt, while an acid was used as the base/solvent.

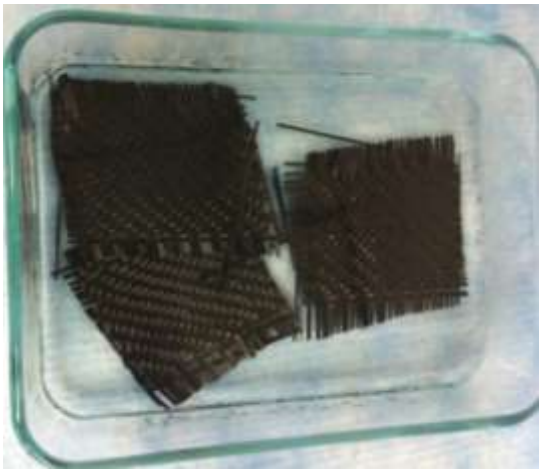

Figure 6.2.1. Carbon fiber mats in immersed in methanol.

In comparison to using tin chlorides as the salt, this method reduces the risk of having residual ions from the acid/solvent (particularly chlorine) being left on the surface and influencing the changes in optical properties. Figure 6.2.1 shows a set of carbon fiber mats in a glass dish immersed in methanol. 3 inch x 3 inch squares of 0°/90° woven carbon fiber mats were immersed in a methanol and acetone wash for 30 minutes, to remove any post manufacturing coating. Figure 6.2.2 shows a carbon fiber mat in a petri dish after being washed in methanol and acetone.

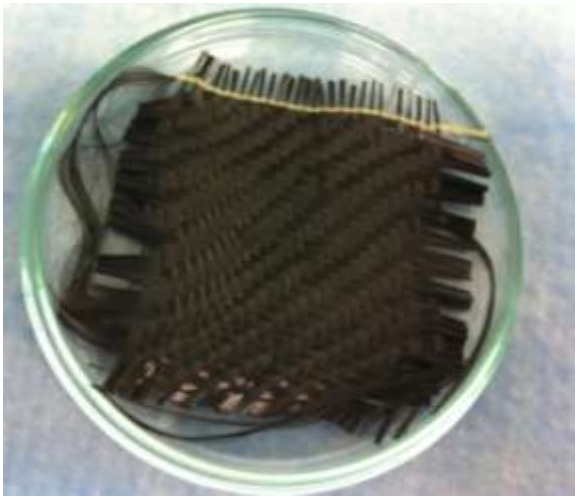

Figure 6.2.2. Uncoated carbon fiber after methanol/acetone wash.

The fiber mats were allowed to dry in air for 2 hours and where then immersed in 2 mL of the ATO solution. After 2 hours of immersion, the fibers where then heat treated in a programmable oven (120 volts/ 12 amps) at 250 °C at atmospheric pressure. In each heat treatment, the temperature was increased to 75 °C for one hour and then increased until 250 °C was reached, to induce the slow removal of the solvent and decrease the possibility of combustion. This step was also implemented to increase the sol-gel layer

quality. Once reached, the specified maximum temperature was held for 1 hour. The samples were allowed to cool to room temperature for a minimum of 4 hours before testing. Figure 6.2.3 shows the sol-gel coated glass slides in the bi-static angular dependent FT-IR spectroscopy sample holder.

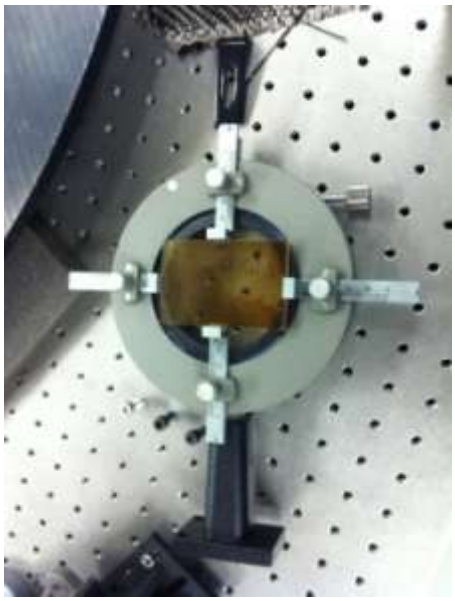

Figure 6.2.3. ATO(Co_2O_3) sol-gel coated quarts slide in the optics sample holder for bi-static angular-dependent transmittance measurements.

4 inch x 2 inch quartz slides were also prepared using the same procedure for transmittance tests discussed below with the optical analysis results. Hemispherical measurements were conducted on an OL-70 Integrating Sphere Reflectance Attachment. A fixed incident angle of 10° was set to measure over a wavelength range of 900 – 1100 nm. A 1" diameter piece of Labsphere 99% spectralon was used as the reflectance standard. For the angular-dependent reflectance, a Bio-Rad FTS 6000 FTIR system was modified to use the embedded Nd:YAG laser (1.064 μm). Two separate experiments

were conducted. First, ATO(x%Co_2O_3) sol-gel coated glass slides were placed at a fixed angle of 0°. This process was completed to investigate the transmittance and reflectivity of the sol-gel coatings independently of the carbon fiber mats. Secondly, the specular angle was found around 90° in respect to the laser source. Once the specular angle was found, the incident angle was altered ± 10° in 5° steps, giving 80°, 85°, 90°, 95°, and 100° incident angle recordings, which is listed in table 6.2.1. For both experiments, the spectra range was set to 0.7-2.3 μm. 32 scan steps were completed on each sample and then integrated into a reading for that particular wavelength.

Table 6.2.1. Measurement angle and correlated degrees from specular angle.

Measurement Angle	Degrees from Specular Angle
80	-10
85	-5
90	0
95	5
100	100

6.3. Results

6.3.1. Hemispherical Reflectance

Three measurements at different spatial locations were made on each sample to account for non-uniformities and defects in the surfaces. These measurements were then averaged to provide the documented reflectance results. Each spectrometer run consists of two modes – comparison and run. Inside the spectrometer system, a mirror is used to rotate in between a specified section of the sphere and the opening where the sample is placed. The detector acts as a photodiode and gives readouts in units of amperage. For

each measurement, a reference measurement is first made from the reflected light, or current, that is collected by the detector. Next, the mirror is switched to reflect light from the sample.

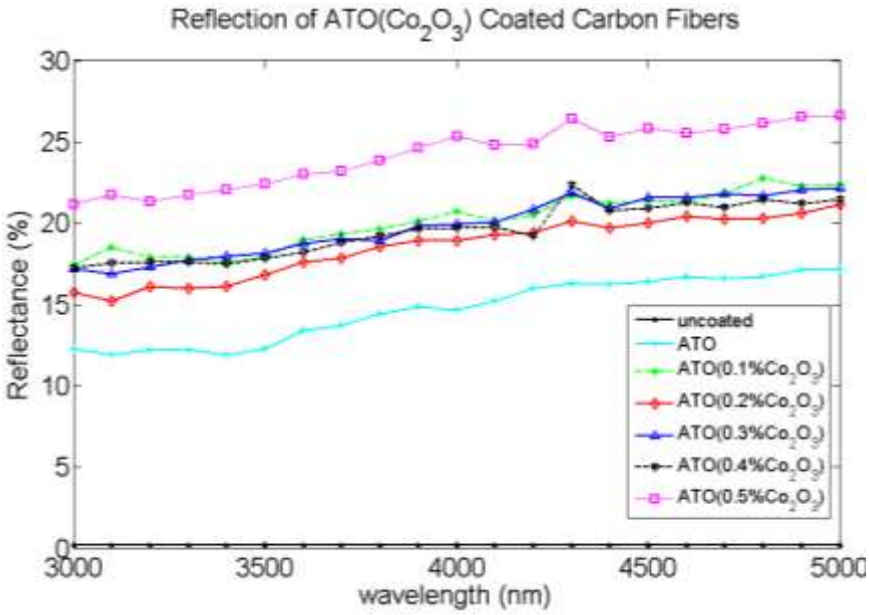

Figure 6.3.1. Hemispherical reflectance of ATO(Co_2O_3) sol-gel coatings on woven carbon fiber mats.

The resulting reflectivity readout is calculated by the ratio of the comparison and run mode amperage readings, giving reflectivity points from 0 to 1. To report the data in terms of percentage, the data points are multiplied by 100. If light passes through the sample, this affects the reading and results in an error. To correct this issue, samples were stacked and placed in a (0°/90°) – (+/-45°) layup scheme to minimize the possibility of light passing through the sample. As seen in figure 6.3.1, the reflectivity increases directly proportional to the increased percentage of Co_2O_3. As hypothesized, the bulk material measurements did not directly correlate to the thin film measurements.

However, the results were comparable to Cheng-Wu et.al. [103] in the 3000 – 5000 nanometer range. As mentioned previously, this range is desired for testing purposes because of the types of thermal infrared detection systems that are used to image aircrafts and missile systems. The 8000 – 12000 nanometer range would be of interest if body temperatures were to be detected.

6.3.2. Angular Dependent Reflectance

The variation in the reflectivity of the samples is seen in figures 6.3.2 through 6.3.7. Figure 6.3.2 shows the reflectance data collected from the sol-gel coated glass slides. Next, the ATO(x%Co_2O_3) sol-gel coated carbon fiber mats were placed in a bi-static detection setup. This means that the signal source was placed at an angle in reference to the detector.

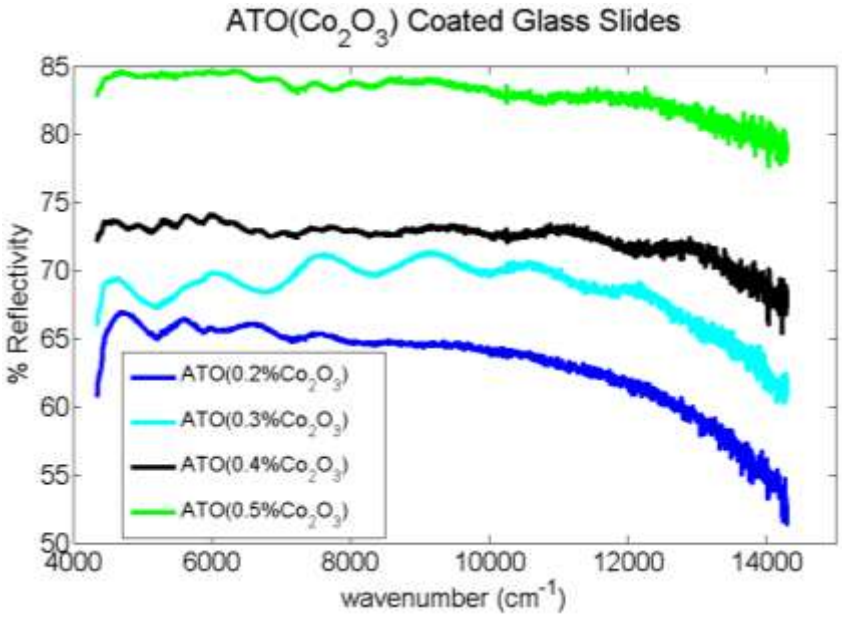

Figure 6.3.2. Reflectance of ATO sol-gel coatings with varying Co_2O_3 doping concentrations.

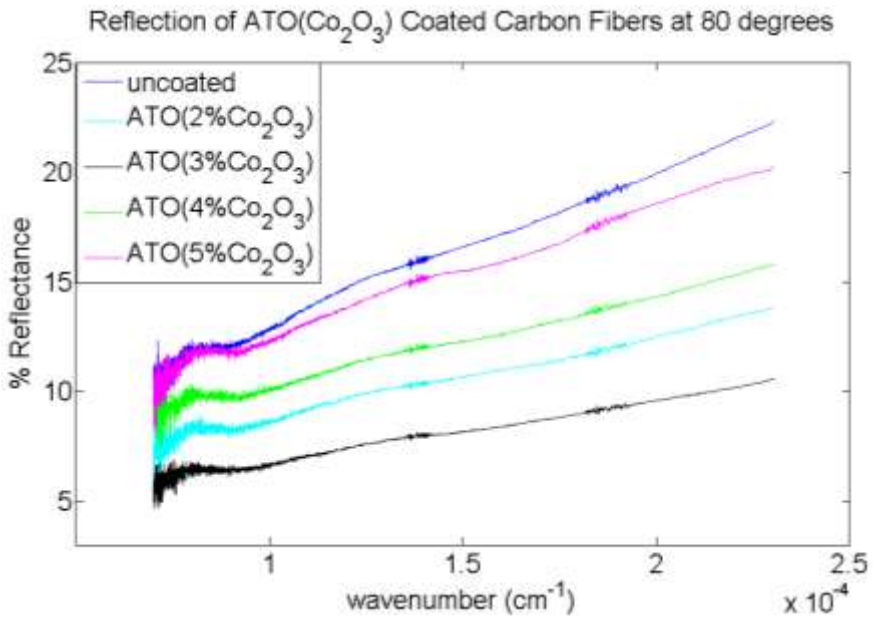

Figure 6.3.3. Reflectance of ATO(x%Co_2O_3) sol-gel coatings with varying Co_2O_3 doping concentrations at an 80° incident angle.

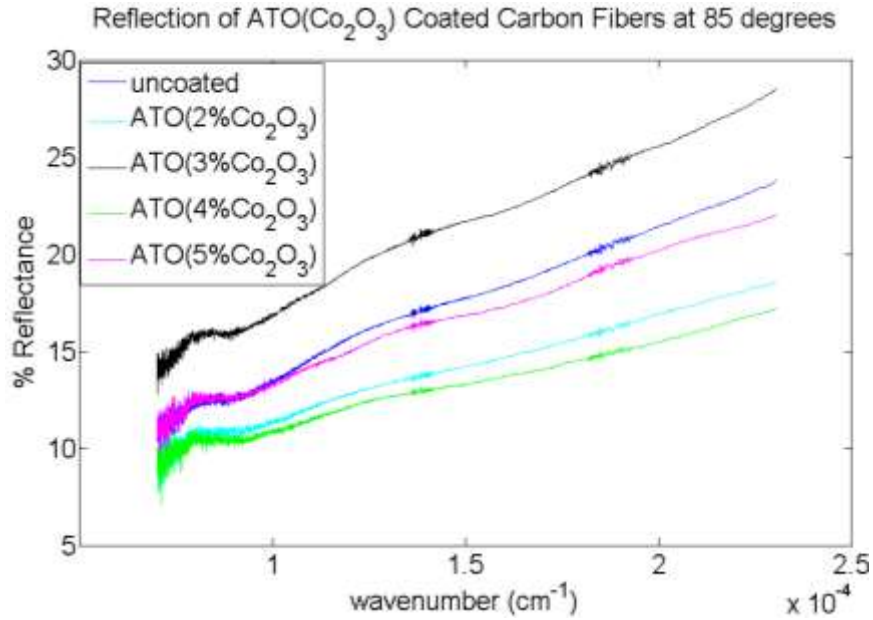

Figure 6.3.4. Reflectance of ATO(x%Co_2O_3) sol-gel coatings with varying Co_2O_3 doping concentrations at an 85° incident angle.

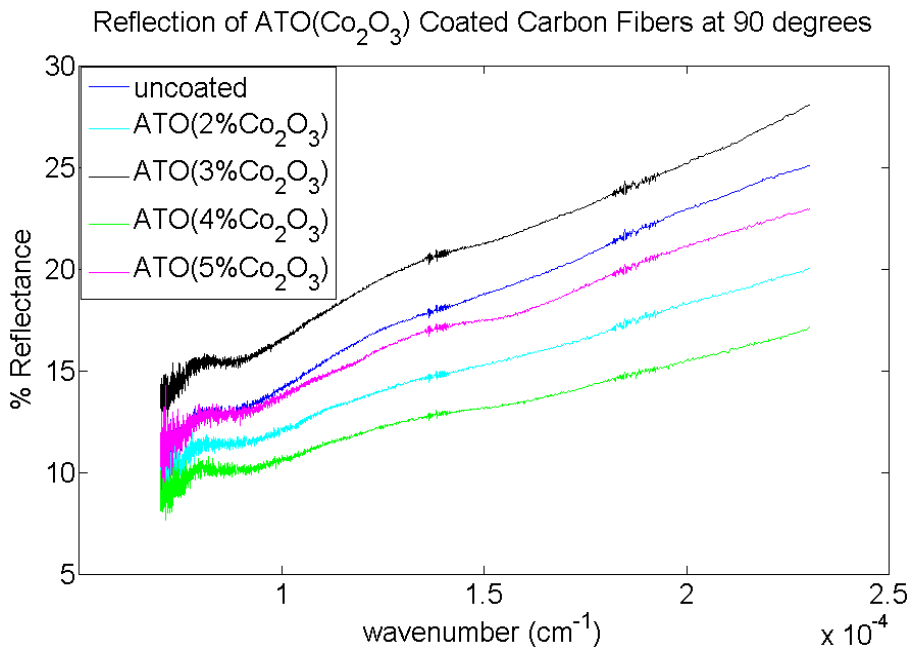

Figure 6.3.5. Reflectance of ATO(x%Co_2O_3) sol-gel coatings with varying Co_2O_3 doping concentrations at a 90° incident angle.

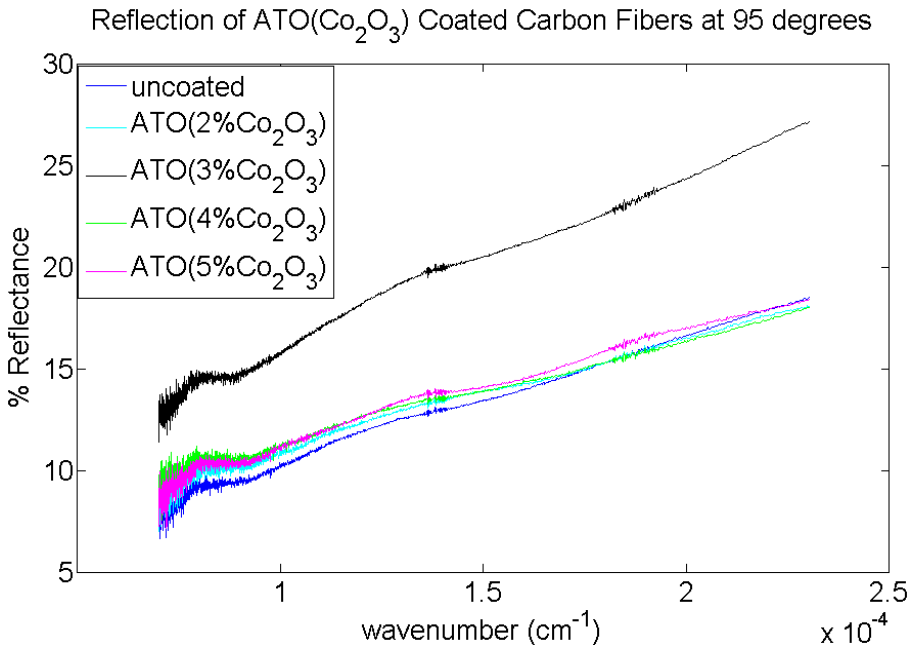

Figure 6.3.6. Reflectance of ATO(x%Co_2O_3) sol-gel coatings with varying Co_2O_3 doping concentrations at an 95° incident angle.

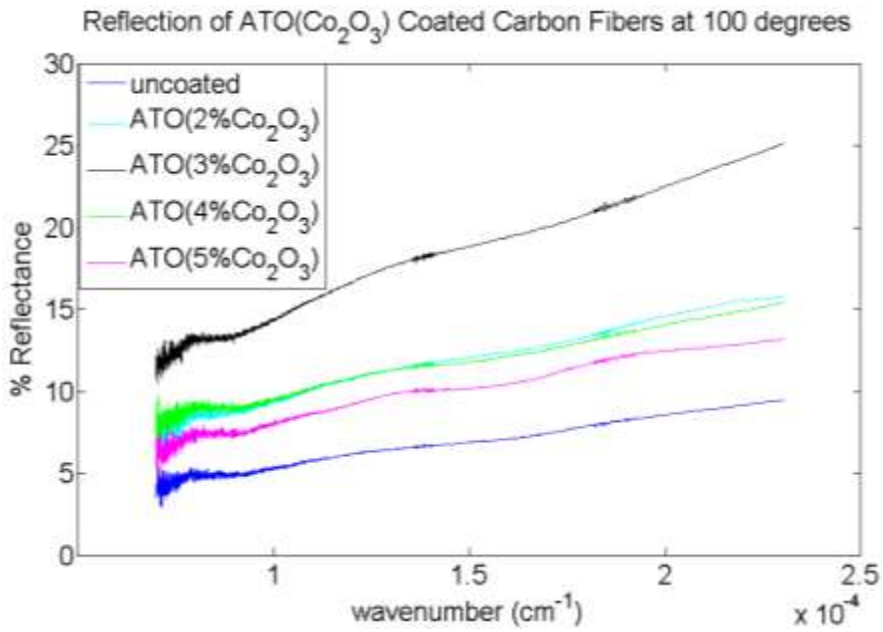

Figure 6.3.7. Reflectance of ATO(x%Co_2O_3) sol-gel coatings with varying Co_2O_3 doping concentrations at an 100° incident angle.

Because of the limitations of the system, the samples were tested in the UV-visible spectrum. In the angle-dependent measurements, the coating of the highest reflectivity varied. This was attributed to the surface roughness and possible thickness variations. The sample size and placement was also taken into consideration during post analysis. Because of the bi-static steup, the beam width stretched from a closely perfect circle with a diameter of ~3 inches to an oval shape with a diameter as wide as ~5 inches.

6.4. Discussion

As seen in figure 6.3.2, thin films of the ATO(x%Co_2O_3) sustain a range of 50-80% reflectivity in the 0.7 to 2.3 μm spectral range. Interestingly, ATO(2%Co_2O_3) approaches 85% reflectivity, giving the highest result. The influence of the added of

Co_2O_3 begins to decrease the reflectivity at doping levels higher than 0.3%. Figures 6.3.3 through 6.3.7 agree with the thin film study that the addition of Co_2O_3 shows the influence of decreased grain growth once doped higher than 0.3%. It is seen from the data that Co_2O_3 doping levels above this limit appear to saturate the ATO and begins to degrade the reflectivity. The beam size of the laser source was roughly three inches in circumference. Because of this, effects from defects in the sol-gel coatings as well as the carbon fiber mat's rigid, conformal surface where negligible. For the hemispherical spectroscopy, the tests were performed at atmospheric pressure in ambient air. Because of this, there was a large dip present in the comparison modes measurements at 4.2 microns. Inside the Au sphere, the standard sample surface was 97 – 98% reflective. The specular plugin was also used to keep the specular component integrated into the diffused component. The calibration baseline of the uncoated carbon fiber mat gave a reflectivity reading of ~0.2%. During the readings, the infrared light source was kept at 6 amperes to reduce the signal to noise ratio. This compensation did not compromise the readings, as we were still considerably high above the noise ground.

When undoped, previous thin film investigations have shown that ATO forms a tetragonal crystal lattice structure. Heat treatments deform this structure, allowing defects and dislocations to populate throughout the crystal. Concurrently, antimony atoms migrate to the surface and increase surface chemistry reactions, thus increasing properties such as conductivity and, particularly, reflectivity. While these Sb ions are migrating to the surface, they cause oxygen vacancies. These excessive oxygen vacancies assist in the atomic alignment of cobalt in tin oxide structures. The changes in reflectivity are attributed to variations of grain growth and ion interactions at the grain

boundaries. From related studies [92] and our previous work [88], it is concluded that Sn ions can be substituted for Sb and Co ions at the grain boundary because of the similar ionic radii (Sn = 0.071 nm, Sb = 0.065 nm, and Co = 0.071 nm). For the effect of the added Co_2O_3, it has been reported that Co can have altered properties based upon the roughness of the carbon surface.[92] From this report, the crystallinity of cobalt varied from the deposition and heat treatment (or curing) process at temperatures as low as room temperature and 250 °C.

6.5. Conclusion

From our results, it is seen that ATO can increase its reflectivity on carbon fiber surfaces when adding less than 0.3% Co_2O_3. This is attributed to a decrease in grain size growth and reactions at the grain boundary. The variations in reflectivity may also be due to agglomerations of the sol-gel coatings in certain parts of the fiber mat, as the surfaces were not perfectly flat, and the fibers have conformal surfaces. However, surface morphology effects were negligible due to the beam size of 3 inches. It is possible that a distinctive correlation can be made by evaluating the conductivity and the magnetic properties coercivity to the doping levels of Co_2O_3.

CHAPTER 7

CONCLUSION

7.1. Summary

This research has presented the implementation and fabrication limits of a novel ferromagnetic/metal oxide sol-gel combination to reflect thermal infrared radiation. The long term goal of this work is to produce a material that will minimize the possible laser induced damage of a material when ablated with infrared 1 – 3 μm laser sources. This application was presented by the Air Force Research Laboratories and associated employees. From the literature review, materials used for similar applications were identified. This allowed materials of interest to be investigated for maximum output. The theory and implementation of ferromagnetic oxides with metal oxides to increase the reflectivity was also identified. A review on currently used carbon fiber composite fabrication techniques showed the vacuum-assisted resin transfer molding technique was identified as the best process to implement this novel material into. This work demonstrates the design and fabrication considerations for sol-gel based thermal infrared reflective coatings for multifunctional carbon fiber composite systems. A two-stage approach was performed to validate theoretical conjectures and confirm experimental

contributions. First, thin films of undoped ATO and cobalt-doped ATO were deposited as a thin film. Standard optical, chemical, and imaging characterizations were performed by FT-IR, Raman spectroscopy, SEM, and EDS. Next, the sol-gels were deposited onto carbon fiber mats for full-scale testing of the bulk materials.

First, investigation and validation of ATO sol-gel thin films for increased infrared reflectivity was performed. In these experiments, silicon wafers were sputtered with carbon and then spin coated with ATO sol-gels. The thin films were then heat treated at various temperatures, ranging from 100 – 500 °C. It was shown that the infrared reflectivity increases based upon the heat treatment temperature. However, the limit for maximum reflectivity was identified by Raman and FT-IR spectroscopy to be 300 °C. The explanation for this effect was attributed to the increased growth of the grain boundaries in the sol-gel layer. In addition, the substitution of Sb^{3+} and Sb^{5+} ions in Sn defects in the crystal lattice occurred, causing the increase in reflectivity.

In the addition of Co_2O_3, sol-gel solutions of ATO and ATO(Co_2O_3) were spin coated onto carbon/silicon substrates. From the extensive literature review, it was confirmed that the oxygen atoms still performed as the charge carriers as it migrated through the sol-gel layer. The increased reflectivity was still attributed to the grain boundary growth. Concurrently, the substitution of Sn^{+2} atom defects and vacancies were substituted by Sb^{3+}, Sb^{5+}, Co^{2+}, and Co^{3+} ions. While increased heat treatment temperatures on undoped ATO sol-gels correlated to an increase in reflectivity between 85 – 90 %, the inclusion of 0.1% Co_2O_3 showed an increase in reflectivity up to 94 %. The ion substitution was proven by Raman spectroscopy investigations. In the spectra, is was observed that Co_2O_3 had a constant level of reflectivity, regardless of the heat

treatment temperatures up to 500 °C. However, the ATO(Co_2O_3) thin film showed higher reflectivity up to 400 °C when compared to the undoped ATO thin film.

In the second stage of investigation, the reflectivity of ATO sol-gels were doped in various levels of Co_2O_3 in the range of 0.1 – 0.5%. The percentage level was kept low due to previous literature already identifying a low Co_2O_3 doping limit of 7% producing higher reflectivity. The secondary purpose was to identify the minimal amount of Co_2O_3 needed to still maximize infrared reflectivity. The coated carbon fibers were then heat treated at 250 °C, because of previous results and previous literature confirmations of heat treatment limitations. Hemispherical integrated reflectance spectroscopy was performed to investigate the absorption and reflection of the sol-gel coatings on carbon fibers.

While it was identified that one coating was not enough to stop the carbon fibers from dominating the absorption of infrared light, two coatings proved to be enough to get high levels of thermal infrared reflection. The specular and diffuse components of reflectivity were integrated together in the plot shown in chapter 6. In addition, angular-dependent bi-static transmittance spectroscopy was performed. From these experiments, it was shown that the specular angle of 90° showed the highest reflectivity. However, ATO(0.3%Co_2O_3) showed the most reflectivity when altered from 80 - 100° of incident infrared radiation. The levels of reflectivity from the sol-gel coated carbon fibers were then compared with thin film results. It was noticed that the angles closest to the specular angle, 85° and 95° showed the most comparable results, still resulting in 80 – 85% reflectivity and 15 – 20% transmittance. Because of the results obtained from this experiment, a qualitative analysis of the effect of number of coating layers versus the

optical response is suggested. This suggested experiment is also mentioned in the future work section.

7.2. Recommendations for Future Work

To extend the limitations of this work, higher and more specific levels of Co_2O_3 doping levels can be identified and tested. However, due to previous literature, it is not expected that the Co_2O_3 doping levels will exceed past 10%. In addition, slightly higher limits on the heat treatment of the sol-gel thin films and coated carbon fibers may yield varying results. The grain boundaries may have more room to grow, and it may compensate for the addition of more Co ions into the structure, as the Sb ions migrate towards the surface. Also, previous literature showed that the Co_2O_3 level of infrared reflectivity could be altered by the roughness of the carbon surface. If the carbon fiber surface roughness is improved by its polymer fabrication techniques, alteration in Co_2O_3 infrared reflectivity will occur.

While it was not investigated in this work, the adhesion of the sol-gel to the carbon fibers can be investigated by nano-indentation. This characterization method can identify the strength of adhesion to the carbon fiber surface, as well as the mechanical strength of the sol-gel coating. This is also vital information when implementing coated carbon fibers into the VARTM process. It would notify the fabricator of its fragileness and flexibility. Therefore, with this research results, it is proven that the materials can be used in mainly flat composite designs until further investigations are done on the flexibility of the coating surfaces. Scanning acoustic microscopy and non-contact atomic

force microscopy can be performed to identify micro and nanoscale defects in the coatings. This will cause variations in the reflectivity measurements. Last, a study of the laser interaction with the ATO(x%Co_2O_3) sol-gel coating will further verify how the coating will perform under various laser conditions. The purpose of this experiment is to investigate the laser damage threshold (LIDT) of cobalt-doped antimony-tin-oxide (ATO) sol-gel coatings in carbon fiber composites. This is of interest to the AFRL for current undisclosed military applications. In general, the breakdown time in correlation with the applied laser power in both instances of pulse count and duration time is of interest. This information is to assist in the design of a thermal infrared reflective coating for carbon fiber composites. Furthermore, the information obtained from this report will contribute to the body of knowledge for such materials in multiple applications such as optoelectronics, transparent conductive oxides for solar cells, and light emitting diodes. LIDT is defined as the highest fluence for which no damage has been observed.

Heat treatments applied to the ATO(Co) sol-gel coatings alter their crystallography and optical parameters. It has been reported that increasing temperatures cause the antimony (Sb) atoms to approach the surface, while cobalt (Co) reinforces the interface by the carbon surface. Also, tin (Sn) transverses the medium, leaving dislocations and defects. Sn^{4+}, Sb^{3+}, Sb5+, Co^{3+} and Co^{5+} have similar radii. This causes cobalt and antimony atoms to fill these vacancies in the crystal lattice. It is from this that the hypothesis is formed. From this set of experiments, a correlation between the surface roughness and calculated LIDT to the laser pulse count and duration time is to be obtained. Also, in conjunction with previous reports of ATO and cobalt's optical and structural parameters, data from the following experiments will be collected to calculate

the surface temperatures [2]. That data will then be correlated to the LIDT and surface roughness. ATO is transparent in the visible spectra, absorbing in the UV spectra, and reflective in the near infrared range (0.7 – 1.2 μm). The increase in heat treatment temperatures will decrease defects and dislocations in the sol-gel coating's stoichiometry. A Nd:YAG laser of 1064 nm (1.064 μm) pulsing at 10 ns with a beam width of 100 μm will show that the LIDT will vary around 23 J/cm^2. The resin used to make the composite is predicted to be evaporated by the laser and to not alter the LIDT.

7.3. Outlook for Possible Future Applications

From this work, various applications can be improved. In the novelty of the fabrication method, it is already being pursued to be proven in research that zirconium oxide/silicon carbide sol-gel precursor combinations can produce high temperature coatings for supersonic and hypersonic applications. In initial literature, the possibility of this sol-gel precursor implementation success is identified because of zirconium oxide and silicon carbide's high melting point of ~2700 C. Just as cobalt was shown to increase the reflectivity of ATO thin films, it is presumed that zirconium oxide will have similar effects with silicon carbide. In sol-gel applications, polycarbosilane is used as the precursor for silicon carbide sol-gel thin films. After heat treatments at high temperatures, the thermal breakdown temperatures of this novel sol-gel combination can be identified.

The design of fiber optic cables relies heavily on the physics described in the area of plasmonics. In this field of study, a plasmon, or electron oscillation, can act

independently or be paired up with an excited electron, or photon, to transfer high bit-rate information. Usually, a laser of a specified wavelength is used to bombard the surface of a metal or metal oxide to release electron (wave)/ electron (particle) pairs from the surface of the material. These electron pairs are detected by a correlated system that converts the electron pairs to bit information that can then be further converted to various forms of data. The coatings used in this project would be ideal for this type of application because of its high level of reflectivity. Because fiber optics currently faces challenges with length from transmitter to receiver and signal durability, a coating of high reflectivity would increase the integrity and durability of the sent signal at longer distances.

Also, in the application of laser lenses, the conducted literature review on how lasers work and types of laser windows showed the possible implementation of ATO sol-gel coatings as a possible laser lens coating material. In laser lenses, over 90% of the infrared light generated by its medium is reflected back into the laser source from the exiting mirror before being reflected again and allowed to radiate outside of the laser cavity. In order for this phenomenon to occur, highly reflective materials must be used. Today, materials such as chromium oxide and tin oxide are already used in commercial laser fabrication. Also, similar annealing techniques are used to assist in the conformation of the deposited material to the lens surface. With cobalt-doped ATO having a high infrared reflectivity of up to ~94%, the implementation of this novel material into laser lens coatings would also prove to be beneficial for unconventional laser cavity shapes and uncommon laser medium sources. However, in an effort to produce this type of coating, more angular-dependent transmittance studies will have to

be performed. Also, another deposition method, such as the dip coating method, will have to be altered in order to assist in uniform coverage of the conformal lens.

New applications such as ferroelectric composite systems are currently being designed in an effort to control the shape of aerospace vehicle panels based on the electromagnetic signal placed on the structure. The overall objective of this application is to control the direction and tilt of an aerospace vehicle. Different multifunctional materials, such as sheets of carbon nanotubes and magnetic materials, are currently being evaluated for their electrical, magnetic, and mechanical strengths to control a composite panel of various layers. Because of the elements present in ATO(Co_2O_3), this application could possibly advance its progress. As previously stated, the resistivity of ATO decreases with heat treatment, which validates carrier mobility enhancement. Also, it has been reported that Co_2O_3 has excellent ferromagnetic properties, as its coercivity can be varied by deposition methods. The increase in carrier mobility and charge density would allow the electromagnetic signals to be processed quicker at longer distances, similar to the advantage for fiber optics applications. Also, stress and strain to the surfaces of the materials during the conforming of the surface would improve with the use of the sol-gel technique. However, just as in this research, multiple coating processes would require monitoring for cracks, defects, and micro-strains to the surface. Also, it is recommended that the investigation of the coatings undergo thin film analysis prior to composite implementation to assure the quality of the sol-gel layers. This would also allow characterization with multiple systems at the nano and bulk scale, as opposed to ruling out certain test methods because of the conformal surface of the the composite system.

REFERENCES

1. Mrinal Kanti Bhowmik, K.S., Sharmistha Majumder, Goutam Majumder, Ashim Saha, Aniruddha Nath Sarma, Debotosh Bhattacharjee, Dipak Kumar Basu and Mita Nasipuri, Thermal Infrared Face Recognition – a Biometric Identification Technique for Robust Security System, P.M. Corcoran, Editor 2011: http://www.intechopen.com/books/reviews-refinements-and-new-ideas-in-face-recognition/thermal-infrared-face-recognition-a-biometric-identification-technique-for-robust-security-system. p. 32.

2. Kruschwitz, J.D.T. and W.T. Pawlewicz, Optical and durability properties of infrared transmitting thin films. Applied Optics, 1997. 36(10): p. 2157-2159.

3. Mohelnikova, J., Materials for reflective coatings of window glass applications. Construction and Building Materials, 2009. 23(5): p. 1993-1998.

4. Mikols, W.J., et al., Evaluation of structural-changes in epoxy systems by moisture sorption-desorption and dynamic mechanical studies. Polymer Composites, 1982. 3(3): p. 118-124.

5. Zaereth, SSY1 Military Surplus Nd-YAG Laser Firing, in wikipedia.org, F.S.M.S.N.-Y.L. Firing, Editor 2009, Zaereth: http://en.wikipedia.org/wiki/File:SSY1_Military_Surplus_Nd-YAG_Laser_Firing.JPG.

6. Kilroy, J.P., C.M.O. Brdaigh, and C.O.A. Semprimoschnig, Mechanical and physical evaluation of new carbon fibre/peek composites for space applications. Sampe Journal, 2008. 44(3): p. 22-34.

7. Mills, A.R. and J. Jones, Investigation, manufacture, and testing of damage-resistant airframe structures using low-cost carbon fibre composite materials and manufacturing technology. Proceedings of the Institution of Mechanical Engineers Part G-Journal of Aerospace Engineering, 2010. 224(G4): p. 489-497.

8. Kim, J.C., O.Y. Kwon, and Z.H. Lee, Unidirectional magnetostrictive Terfenol/epoxy composite. Applied Physics Letters, 2004. 84(12): p. 2130.

9. Giurgiutiu, V. and K.L. Reifsnider, Development of strength theories for random fiber composites. Journal of Composites Technology & Research, 1994. 16(2): p. 103-114.

10. Cho, J., et al., Carbon nanotubes: do they toughen brittle matrices? Journal of Materials Science, 2011. 46(14): p. 4770-4779.

11. Feraboli, P., et al., Defect and damage analysis of advanced discontinuous carbon/epoxy composite materials. Composites Part A: Applied Science and Manufacturing, 2010. 41(7): p. 888-901.

12. Feraboli, P., et al., Characterization of Prepreg-Based Discontinuous Carbon Fiber/Epoxy Systems. Journal of Reinforced Plastics and Composites, 2008. 28(10): p. 1191-1214.

13. Hu, Z.-g. and Y. Zhang, Continuum damage mechanics based modeling progressive failure of woven-fabric composite laminate under low velocity impact. Journal of Zhejiang University SCIENCE A, 2010. 11(3): p. 151-164.

14. Im, J.S., et al., Effect of heat treatment on ZrO2-embedded electrospun carbon fibers used for efficient electromagnetic interference shielding. Journal of Physics and Chemistry of Solids, 2011. 72(10): p. 1175-1179.

15. Micheli, D., et al., Nanostructured composite materials for electromagnetic interference shielding applications. Acta Astronautica, 2011. 69(9-10): p. 747-757.

16. Gupta, A., et al., Mechanism and kinetics of the curing process in the tgddm-dds resin system. Abstracts of Papers of the American Chemical Society, 1984. 187(APR): p. 15-INDE.

17. Nam, I.W., H.K. Lee, and J.H. Jang, Electromagnetic interference shielding/absorbing characteristics of CNT-embedded epoxy composites. Composites Part A: Applied Science and Manufacturing, 2011. 42(9): p. 1110-1118.

18. Featherston, M., F-22 arrives at Joint Base Pearl Harbor Hickam, Hawaii, H. Public domain - F-22 arrives at Joint Base Pearl Harbor Hickam, Editor 2010: http://www.thepublicdomain.net/2010/07/f-22-arrives-at-joint-base-pearl-harbor.html. p. F-22 Raptor Fighter Jet.

19. Thakre, P.R., et al., Investigation of the effect of single wall carbon nanotubes on interlaminar fracture toughness of woven carbon fiber--epoxy composites. Journal of Composite Materials, 2011. 45(10): p. 1091-1107.

20. Trapalis, C.C., et al., Study of a multilayer wavelength-selective reflector prepared by the sol-gel process. Materials Letters, 1995. 25(5–6): p. 265-269.

21. Lavers, C.R., et al., Planar optical waveguides for sensing applications. Sensors and Actuators B-Chemical, 2000. 69(1-2): p. 85-95.

22. Sun, M., W. Que, and X. Hu, Preparation and optical properties of sol–gel derived organic–inorganic hybrid waveguide films doped with disperse red 1 azoaromatic chromophores. Optical Materials, 2009. 32(1): p. 49-53.

23. Babar, A.R., et al., Sensing properties of sprayed antimony doped tin oxide thin films: Solution molarity. Journal of Alloys and Compounds, 2011. 509(6): p. 3108-3115.

24. Benrabah, B., et al., Impedance studies of Sb doped SnO2 thin film prepared by sol gel process. Superlattices and Microstructures, 2011. 50(6): p. 591-600.

25. Carlesi Jara, C., et al., Improving the stability of Sb doped Sn oxides electrode thermally synthesized by using an acid ionic liquid as solvent. Chemical Engineering Journal, 2011. 171(3): p. 1253-1262.

26. Castro, M.R.S., P.W. Oliveira, and H.K. Schmidt, Enhanced mechanical and electrical properties of antimony-doped tin oxide coatings. Semiconductor Science and Technology, 2008. 23(3): p. 035013.

27. Dua, L.K., et al., Study of spin coated high antimony content Sn–Sb oxide films on silica glass. Materials Characterization, 2008. 59(5): p. 578-586.

28. Biswas, P.K., et al., Effects of tin on IR reflectivity, thermal emissivity, Hall mobility and plasma wavelength of sol–gel indium tin oxide films on glass. Materials Letters, 2003. 57(15): p. 2326-2332.

29. Senguttuvan, T.D. and L.K. Malhotra, Sol gel deposition of pure and antimony doped tin dioxide thin films by non alkoxide precursors. Thin Solid Films, 1996. 289(1–2): p. 22-28.

30. Shanthi, S., C. Subramanian, and P. Ramasamy, Growth and characterization of antimony doped tin oxide thin films. Journal of Crystal Growth, 1999. 197(4): p. 858-864.

31. Zhu, Y.C. and J.S. Jiang, Synthesis and characterization of alpha-fe2o3@ato nanocomposite particles. Surface Review and Letters, 2008. 15(5): p. 545-550.

32. Lussier, A., et al., Comparative x-ray absorption spectroscopy study of Co-doped SnO[sub 2] and TiO[sub 2]. Journal of Applied Physics, 2004. 95(11): p. 7190-7191.

33. Chen, X.C., Synthesis and characterization of ATO/SiO2 nanocomposite coating obtained by sol-gel method. Materials Letters, 2005. 59(10): p. 1239-1242.

34. Iga, K., Fundamentals of Laser Optics, 1994, Plenum Press: New York. p. 1-231.

35. Tsallis, C., Generalization of the Planck radiation law and application to the cosmic microwave background radiation. Physical review. B, Condensed matter, 1995. 52(2): p. 1447.

36. Batzill, M. and U. Diebold, The surface and materials science of tin oxide. Progress in Surface Science, 2005. 79(2-4): p. 47-154.

37. Harrison, P.G. and B. Maunders, Tin oxide surfaces. Part 15.?Infrared study of the adsorption of propene on tin(IV) oxide, tin(IV) oxide?silica and tin(IV) oxide?palladium oxide. Journal of the Chemical Society, Faraday Transactions 1, 1985. 81(6): p. 1329.

38. Shanthi, E., et al., Electrical and optical-properties of tin oxide-films doped with F and (SB+F). Journal of Applied Physics, 1982. 53(3): p. 1615-1621.

39. Zhurbina, I.A., O.I. Tsetlin, and V.Y. Timoshenko, Optical generation of free charge carriers in thin films of tin oxide. Semiconductors, 2011. 45(2): p. 236-240.

40. Yahaya, M., M.M. Salleh, and I.A. Talib, Optical properties of MoO3 thin films for electrochromic windows. Solid State Ionics, 1998. 113–115(0): p. 421-423.

41. Zhong, X., et al., Effect of calcining temperature and time on the characteristics of Sb-doped SnO2 nanoparticles synthesized by the sol–gel method. Particuology, 2012. 10(3): p. 365-370.

42. Baklanova, N.I., et al., Protective ceramic multilayer coatings for carbon fibers. Surface and Coatings Technology, 2006. 201(6): p. 2313-2319.

43. Bichurin, M.I., D. Viehland, and G. Srinivasan, Magnetoelectric interactions in ferromagnetic-piezoelectric layered structures: Phenomena and devices. Journal of Electroceramics, 2007. 19(4): p. 243-250.

44. Park, K.-Y., et al., Microwave absorbing hybrid composites containing Ni–Fe coated carbon nanofibers prepared by electroless plating. Composites Part A: Applied Science and Manufacturing, 2011. 42(5): p. 573-578.

45. Xu, J., et al., Preparation and characterization of carbon fibers coated by Fe3O4 nanoparticles. Materials Science and Engineering: B, 2006. 132(3): p. 307-310.

46. Zhai, J., et al., Magnetoelectric Laminate Composites: An Overview. Journal of the American Ceramic Society, 2008. 91(2): p. 351-358.

47. Zima, T.M., N.I. Baklanova, and A.T. Titov, Ferromagnetic composite coatings on carbon fibers. Inorganic Materials, 2011. 47(4): p. 385-389.

48. Łączka, M. and K. Cholewa, Chromium, cobalt, nickel and copper as pigments of sol-gel glasses. Journal of Alloys and Compounds, 1995. 218(1): p. 77-85.

49. Pillonnet, A., et al., Fluorescence of Cr3+ doped alumina optical waveguides prepared by pulsed laser deposition and sol–gel method. Journal of Luminescence, 2000. 87–89(0): p. 1087-1089.

50. Growth and characterization of antimony doped tin oxide thin films. Journal of Crystal Growth, 1999. 197. p. 858-864.

51. Electrochromism of nanoparticulate-doped metal oxides: optical and material properties. Displays. 20: p. 145-154.

52. E. Shanthi, V.D., A. Banerjee, K. L. Chopra, Electrical and optical properties of undoped and antimony-doped tin oxide films. Journal of Applied Physics, 1980. 51(12).

53. Koji Tsukuma, T.A., Hiroaki Imai, Hydrolysis deposition of thin films of antimony-doped tin oxide. Journal of American Ceramic Society, 2001. 84(4): p. 869-871.

54. Seo, M., Y. Akutsu, and H. Kagemoto, Preparation and properties of Sb-doped SnO2/metal substrates by sol–gel and dip coating. Ceramics International, 2007. 33(4): p. 625-629.

55. Dušek, K., Network formation in curing of epoxy resins, in Epoxy Resins and Composites III, K. Dušek, Editor. 1986, Springer Berlin Heidelberg. p. 1-59.

56. Benrabah, B., et al., Sol-gel preparation and characterization of antimony doped tin oxide (ATO) powders and thin films. The European Physical Journal Applied Physics, 2009. 48(3): p. 30301.

57. Geraldo, V., et al., Drude's model calculation rule on electrical transport in Sb-doped SnO2 thin films, deposited via sol-gel. Journal of Physics and Chemistry of Solids, 2006. 67(7): p. 1410-1415.

58. Wei, P., H. Xiaowei, and C. Yan, Preparation and Characterization of Poly (vinyl alcohol)/Antimony-Doped Tin Oxide Nanocomposites. International Journal of Polymeric Materials, 2010. 60(3): p. 223-232.

59. Lee, S.Y. and B.O. Park, Structural, electrical and optical characteristics of SnO2 : Sb thin films by ultrasonic spray pyrolysis. Thin Solid Films, 2006. 510(1-2): p. 154-158.

60. Stjerna, B., E. Olsson, and C.G. Granqvist, Optical and electrical properties of radio frequency sputtered tin oxide films doped with oxygen vacancies, F, Sb, or Mo. Journal of Applied Physics, 1994. 76(6): p. 3797.

61. Ravichandran, K. and P. Philominathan, Analysis of critical doping level of sprayed antimony doped tin oxide films. Journal of Materials Science: Materials in Electronics, 2010. 22(2): p. 158-161.

62. Liu, J., et al., Novel Single-Crystalline Hierarchical Structured ZnO Nanorods Fabricated via a Wet-Chemical Route: Combined High Gas Sensing Performance with Enhanced Optical Properties. Crystal Growth & Design, 2009. 9(4): p. 1716-1722.

63. Geraldo, V., et al., Drude's model calculation rule on electrical transport in Sb-doped SnO2 thin films, deposited via sol–gel. Journal of Physics and Chemistry of Solids, 2006. 67(7): p. 1410-1415.

64. Saadeddin, I., et al., Synthesis and characterization of single- and co-doped SnO2 thin films for optoelectronic applications. Applied Surface Science, 2007. 253(12): p. 5240-5249.

65. Tsuzuki, T., K. Pethick, and P.G. McCormick, Synthesis of CaCO3 nanoparticles by mechanochemical processing. Journal of Nanoparticle Research, 2000. 2(4): p. 375-380.

66. Music, S., et al., Formation of chromia from amorphous chromium hydroxide. Croatica Chemica Acta, 1999. 72(4): p. 789-802.

67. Wang, X., et al., Effect of antimony doped tin oxide on behaviors of waterborne polyurethane acrylate nanocomposite coatings. Surface & Coatings Technology, 2010. 205(7): p. 1864-1869.

68. Szczuko, D., et al., XPS investigations of surface segregation of doping elements in SnO2. Applied Surface Science, 2001. 179(1–4): p. 301-306.

69. Xu, C.N., et al., Stabilization of sno2 ultrafine particles by additives. Journal of Materials Science, 1992. 27(4): p. 963-971.

70. Jiang, Y.-c.Z.a.J.-s., Synthesis and characterization of alpha-Fe2O3@ATO nanocomposite particles. Surface Review and Letters, 2007. 15(5): p. 545-550.

71. V. Teixeira, E.S., M. F. Costa, C. Nunes, L. Rosa, M. J. Carvalho, M. Collares-Pereira, E. Roman, J. Gago, Spectrally selectivy composite coatings of Cr-Cr2O3 and Mo-Al2O3 for solar energy applications. Thin Solid Films, 2001. 392: p. 320-326.

72. Götzendörfer, S. and P. Löbmann, Influence of single layer thickness on the performance of undoped and Mg-doped CuCrO2 thin films by sol–gel processing. Journal of Sol-Gel Science and Technology, 2010. 57(2): p. 157-163.

73. Muraoka, Y., N. Takubo, and Z. Hiroi, Photoinduced conductivity in tin dioxide thin films. Journal of Applied Physics, 2009. 105(10): p. 103702.

74. Singh, M.K., M.C. Mathpal, and A. Agarwal, Optical properties of SnO2 quantum dots synthesized by laser ablation in liquid. Chemical Physics Letters, 2012. 536: p. 87-91.

75. Hilary Uche Igwe, E.I.U., Optical characteristics of nanocrystalline thermal annealed tin oxide thin film samples prepared by chemical bath deposition technique. Advances in Applied Science Research, 2010. 1(3): p. 240-246.

76. T. D. Senguttuvan, L.K.M., Sol gel deposition of pure and antimony doped tin dioxide thin films by non alkoxide precursors. Thin Solid Films, 1996. 289: p. 22-28.

77. Sung-Soon Park, H.Z., J. D. Mackenzie, Sol-gel derived antimony-doped tin oxide coatings on ceramic cloths. Materials Letters, 1994. 22: p. 175-180.

78. V. Geraldo, V.B., L. V. A. Scalvi, C. V. Santilli, Structural characterization of nanocrystalline Sb-doped SnO2 xerogels by multiedge X-ray absorption spectroscopy. Journal of Physical Chemistry C, 2010. 114: p. 19206-19213.

79. Krishnakumar, T., et al., Structural, optical and electrical characterization of antimony-substituted tin oxide nanoparticles. Journal of Physics and Chemistry of Solids, 2009. 70(6): p. 993-999.

80. Mishra, K., K. Johnson, and P. Schmidt, Electronic structure of antimony-doped tin oxide. Physical Review B, 1995. 51(20): p. 13972-13976.

81. Greber, T., Probing the Electronic States of Band Ferromagnets with Photoemission, in Band Ferromagnetism: Ground-state and Finite-temperature Phenomena. 2001, Springer: Verlag Berlin Heidelberg. p. 95-109.

82. Drasovean, R., et al., Optical properties of cobalt oxide films by a dipping sol–gel process. Journal of Non-Crystalline Solids, 2006. 352(9–20): p. 1479-1485.

83. Senthilkumar, V., et al., Effects of annealing temperature on structural, optical, and electrical properties of antimony-doped tin oxide thin films. Philosophical Magazine Letters, 2010. 90(5): p. 337-347.

84. Montero, J., C. Guillén, and J. Herrero, Discharge power dependence of structural, optical and electrical properties of DC sputtered antimony doped tin oxide (ATO) films. Solar Energy Materials and Solar Cells, 2011. 95(8): p. 2113-2119.

85. Maghanga, C.M., et al., Transparent and conducting TiO2:Nb films made by sputter deposition: Application to spectrally selective solar reflectors. Solar Energy Materials and Solar Cells, 2010. 94(1): p. 75-79.

86. Babar, A.R., et al., Structural and optoelectronic properties of antimony incorporated tin oxide thin films. Journal of Alloys and Compounds, 2010. 505(2): p. 416-422.

87. Rastomjee, C.S., et al., Infrared reflectance spectra of Sb-doped SnO2 ceramics. Journal of Materials Chemistry, 1991. 1(3): p. 451.

88. B. Richard, N.A., S. Thomas, Cobalt-Doped Antimony-Tin Oxide Sol-Gels on Carbon-Silicon Layers for Modeling Sol-Gel-Carbon Fiber Interfaces. Japanese Journal of Applied Physics, 2012. 51: p. 11-15.

89. Kim, Y.C., et al., Effect of Sb doping on the opto-electronic properties of SnO2 nanowires. Thin Solid Films, 2012. 520(21): p. 6471-6475.

90. Pal, J. and P. Chauhan, Study of physical properties of cobalt oxide (Co3O4) nanocrystals. Materials Characterization, 2010. 61(5): p. 575-579.

91. Ma, J., et al., UV–violet photoluminescence emitted from SnO2:Sb thin films at different temperature. Materials Letters, 2005. 59(17): p. 2142-2145.

92. Shi, J., M. Azumi, and O. Nittono, Structural and magnetic properties of Co-C composite films and Co/C multilayer films. Applied Physics A Materials Science & Processing, 2001. 73(2): p. 215-218.

93. Teixeira, V., et al., Spectrally selective composite coatings of Cr–Cr2O3 and Mo–Al2O3 for solar energy applications. Thin Solid Films, 2001. 392(2): p. 320-326.

94. Teixeira, V., et al., Chromium-based thin sputtered composite coatings for solar thermal collectors. Vacuum, 2002. 64(3–4): p. 299-305.

95. Sun, K., et al., Effect of the heat treatment on the infrared emissivity of indium tin oxide (ITO) films. Applied Surface Science, 2011. 257(22): p. 9639-9642.

96. Chao, Y., W. Tang, and X. Wang, Properties of Resistivity, Reflection and Absorption Related to Structure of ITO Films. Journal of Materials Science & Technology, 2012. 28(4): p. 325-328.

97. Conti, T.G., et al., Electrical Properties of Highly Conducting SnO2:Sb Nanocrystals Synthesized using a Nonaqueous Sol-Gel Method. Journal of the American Ceramic Society, 2010. 93(11): p. 3862-3866.

98. Mattox, D., Handbook of Vapor Deposition. 2010, Noyes Publications: Westwood, New Jersey. p. 383-384.

99. Zhang, J. and L. Gao, Synthesis and characterization of antimony-doped tin oxide (ATO) nanoparticles. Inorganic Chemistry Communications, 2004. 7(1): p. 91-93.

100. Wu, F.D., M. Wu, and Y. Wang, Antimony-doped tin oxide nanotubes for high capacity lithium storage. Electrochemistry Communications, 2011. 13(5): p. 433-436.

101. Chan, J.C., et al., Mechanisms of Aging of Antimony Doped Tin Oxide Based Electrochromic Devices. Japanese Journal of Applied Physics, 2006. 45(No. 49): p. L1300-L1303.

102. Zu, X.T., et al., Comparative studies of laser-induced damage of several single-layer optical films. Nuclear Instruments and Methods in Physics Research Section B: Beam Interactions with Materials and Atoms, 2008. 266(12-13): p. 3195-3199.

103. Fu, C.W., S.Q. Zhang, and M.Q. Chen, Investigation on the thermal radiation properties of antimony doped tin oxide particles. Chinese Physics B, 2008. 17(3): p. 1107-1112.

ABOUT THE AUTHOR

The author received his bachelor degree in electrical engineering from Southern University A&M of Baton Rouge, Louisiana in 2009. He then received his masters degree in electrical engineering from the University of South Florida in Tampa, Florida in 2011. During his graduate studies, he conducted research with the Advanced Materials and Biocompatible Interfaces Research (AMBIR) Group, where he managed several research projects, stemming from electrospinning, solar cell fabrication, and carbon fiber composite coatings. For his doctoral research, he conducted research in conjunction with the Air Force Research Laboratory in Eglin Air Force Base. This research involved the integration of advanced materials for increasing functions of carbon fiber reinforced composite systems. His research objective is functionalizing advanced materials for thermal infrared reflectivity and integration into carbon fiber composites. The author's research interests are in the areas of optics, materials science, and solid state physics, and micro/nanofabrication.